Chapter 4 - Waves and Energetic Particles

This page intentionally left blank

Chapter 4

Waves and Energetic Particles

4.1 Introduction

Spherical torus (ST) discharges, such as those in NSTX, provide a unique opportunity for studying wave-particle interactions in plasma at high β and dielectric constant. In addition, fast ions produced during neutral beam injection in NSTX have velocities that exceed the Alfvén speed and can consequently resonate strongly with a wide variety of Alfvén waves. Controlling the distribution function of energetic ions through phase-space engineering is an important topic for spherical torus physics, as well as for ITER and tokamak research in general.

Scenarios that use high harmonic fast wave (HHFW), electron cyclotron wave (ECW) and electron Bernstein wave (EBW) heating and current drive are being developed and explored in NSTX to assist non-inductive plasma start-up, plasma current ramp-up and sustained plasma operation at high β, through the use of HHFW current drive to control q(0) and HHFW bulk heating. These scenarios will be discussed in detail in Chapter 6.

The 30 MHz HHFW heating and current drive system has been operational on NSTX since its inception. In recent years a deeper understanding of HHFW coupling physics has developed leading to significantly

improved coupling efficiency, with and without neutral beam heating, in L-mode plasmas. This improved coupling has resulted in the production of NSTX record core electron temperatures of over 5 keV with HHFW heating and the first direct measurement of on-axis HHFW current drive. These new results have led to several proposed improvements to the HHFW antenna that will support the 2009 - 2013 research program, and have important implications for future devices, including NHTX, the ST-CTF and ITER. Section 4.2 of this chapter discusses the status of HHFW research and plans for the NSTX HHFW program.

To date the ECW/EBW research program on NSTX has been focused on determining the EBW coupling efficiency for various plasma scenarios via the measurement of thermal EBW emission, and the theoretical modeling of EBW coupling, propagation, heating and current drive. With only baseline funding no EBW heating system is planned for NSTX during the time period covered by this five-year plan. However, a 28 GHz, 350 kW gyrotron is proposed for installation on NSTX in 2011 to support ECH-assisted plasma startup and, with additional incremental funding, installation of second 350 kW 28 GHz gyrotron is proposed in 2012. This 700 kW 28 GHz heating system, in combination with an EBW antenna, would allow the first high power EBW coupling and heating tests on NSTX. Section 4.3 presents the status of EBW research and plans for the NSTX ECW/EBW program.

Energetic particle research on NSTX has yielded important new results, including the discovery of CAE/GAE, Alfvén-acoustic modes, multi-mode transport and a new understanding of chirping modes. These experimental results have helped advance theoretical modeling and have significant implications for future burning plasma devices. Section 4.4 presents the status of energetic particle research and plans for the NSTX energetic particle program. One component of the energetic particle research plan is the study of wave-particle interactions though the use of active antenna excitation of various Alfven eigenmodes observed in NSTX, which would lay the foundation for optimizing the performance of future fusion reactors, including the use of alpha channeling.

Plasma operation at toroidal magnetic fields up to 1 T, after installation of the new center-stack in 2011, will allow an assessment of HHFW physics in a regime where surface wave losses will be significantly reduced and at plasma parameters much closer to next-step STs. Operation at 1 T will also benefit the 28 GHz EBW research program by allowing fundamental resonance EBW heating, which has much better radial access than second harmonic heating. The higher field will also extend the range of $V_{fast}/V_{Alfvén}$ and

r* for scaling studies of the *AE activity, especially for the scaling of TAE avalanches closer to ITER parameters. The addition of the Liquid Lithium Divertor, in combination with the two existing LITER lithium injectors, will provide an important tool to enable improved HHFW and EBW coupling in H-mode plasmas.

4.2 High Harmonic Fast Wave Physics

4.2.1 HHFW Research Goals

The ultimate goals of the HHFW program on NSTX are to enable non-inductive plasma current ramp-up, and to provide q(0) control and bulk heating of H-mode plasmas to support very long pulse non-inductive plasma sustainment at high β [4.2.1]. Research to date has been directed toward understanding the HHFW coupling physics and improving the coupling efficiency for current drive phasing [4.2.2, 4.2.3] and, more recently, the exploration of HHFW current drive in L-mode plasmas [4.2.4]. Considerable improvement in coupling efficiency has been obtained in keeping with fast wave modeling by setting conditions to avoid fast wave propagation too close to the antenna/wall surfaces. It turns out that HHFW propagation is rather strongly directed close to the magnetic field direction, which favors propagation in the surface plasma and thus surface damping. Also, GENRAY [4.2.5] and AORSA [4.2.6] modeling show that the waves inside the plasma tend to be localized to the outer half of the plasma, potentially again favoring surface damping. This latter effect, which is particular to the HHFW regime, may also afford a means of localizing the HHFW power deposition off the axis of the plasma.

The HHFW research goals for 2009-10 will advance the physics basis established for L-mode plasmas to the plasma current ramp-up and H-mode regimes. These goals include:

1. Optimize heating and current drive in the H-mode and plasma ramp-up regime through the use of lithium injection and the Liquid Lithium Divertor to enhance HHFW coupling for plasma current ramp-up and discharge sustainment.
2. Increase the plasma-antenna gap to provide for less interaction of energetic neutral beam ions with the antenna and to permit optimization of the heating/current drive of H-mode plasmas by reducing edge density near the antenna to reduce edge power loss and avoiding arcing and edge MHD

3. Enhance coupled RF power by modifying the antenna to have two feedthroughs per strap and to have lower RF-induced electric fields
4. Include an ELM dump in the matching circuit to better couple to H-modes without arcing and use an electronic feedback system to avoid coupling power during ELMs

The HHFW research goals for 2011-13 support fully non-inductive plasmas with HHFW-assisted current ramp-up and very long pulse plasma operation with an upgraded antenna and HHFW controls that are integrated with the NSTX plasma control system (PCS). This research will benefit from improved coupling at the higher toroidal field that will be possible with the new center-stack in 2012-13. These goals include:

1. Optimizing HHFW heating and current drive in NBI deuterium H-mode conditioned with lithium.
2. Benchmarking current drive results against advanced RF codes.
3. Controlling q on-axis during very long pulse operation.
4. Combining HHFW coupling during current ramp-up with 28 GHz ECH-assisted CHI and PF-only plasma startup to provide fully non-inductive startup.

4.2.2 HHFW Physics

HHFW coupling, propagation and damping physics are important areas of research on NSTX. Each must be understood to properly predict core vs. surface heating as well as the radial profile of the heating and current drive. Extensive theoretical and modeling studies have been and are being carried out to address these three critical areas for NSTX as well as for tokamaks generally. These studies, which are supported by the NSTX Project and by other DOE grants to the PSFC-MIT, CompX Corporation, and the RF SciDAC project, include the following efforts:

1) Analysis of the global 3D structure of the HHFW electric fields, energy flow, and power deposition is under way using both ray tracing [GENRAY] and full wave codes [AORSA, METS, and TORIC]. At the present time, these codes include both linear collisionless and collisional damping mechanisms. However, since experimental results indicate that significant damping may occur in the edge regions due to surface wave propagation, generalized boundary conditions that can treat edge dissipation due to the

formation of RF sheaths near the vacuum vessel wall and launcher are now being developed by the RF SciDAC group for inclusion in the full wave modeling codes.

2) Self-consistent simulations of the HHFW interactions with energetic ions are needed to accurately determine the power deposition and current drive that can be achieved in discharges with co-resonant neutral beam injection (NBI). Experimental observations indicate that the fast ions can interact strongly with HHFW, leading to significant modifications of the fast ion velocity distributions as well as the partitioning of the wave power among the various plasma species. To properly include the effects of these interactions, the wave propagation codes must be coupled with a Fokker-Planck treatment of the ion and electron distribution functions in ST geometry that includes effects of quasilinear diffusion at high cyclotron harmonics, collisions, trapped particle effects, and particle losses. Previously, the main focus of these studies was the GENRAY / CQL3D package, which was used to model the early combined HHFW and NBI experiments on NSTX [4.2.7]. More recently, the 1D and 2D full wave codes have all been generalized to include non-Maxwellian particle distributions in the plasma dielectric response modules. The CQL3D code has been integrated with the AORSA code, and work is currently underway to integrate it with the TORIC code. Since the power deposition and driven current profiles can change significantly as the resonant ion distributions evolve in time, the TORIC code has been integrated into the TRANSP analysis package, and work is currently underway to include CQL3D as well. Work is also underway in the RF SciDAC project to address the effects of finite drift orbit width on power deposition, an effect that may be important in both ST's as well as conventional tokamaks in which RF power damps on energetic ions.

3) In general, wave propagation and deposition codes have simplified models for the wave launcher: the codes assume that the amount of power that is coupled into the plasma is known. However, as the recent experiments on NSTX and previous results from other devices have shown, the core heating efficiency is strongly dependent on the launched wave spectrum as well as the other discharge characteristics. An analysis of the power coupled into the plasma that self-consistently includes the effect of the core absorption and wave propagation dynamics, rather than assuming a radiation boundary condition, is needed to understand the experimental observations on NSTX as well as on other tokamaks, including ITER. As a first step towards the development of this modeling capability, collaborators from the PSFC-

MIT and the RF SciDAC group have been developing an interface between the TOPICA 3D antenna module and the TORIC full wave code. This package, when complete, will be used to analyze the heating profiles in NSTX for various strap phasings on the NSTX launcher. Results from these studies should indicate regimes of operation in which the driven currents can be optimized for plasma start-up, ramp-up, or high performance sustainment phase.

4) The theoretical analysis tools for quantitative, or even semi-quantitative analysis of the parametric decay instability (PDI) phenomenon are not presently available. The AORSA1D all-orders full wave code is being modified to include resonant three-wave interactions. Because AORSA employs a spectral basis set, in essence a complete set of pseudo modes, this modification to account for so-called "extended pump" interactions should be straight forward to implement on a 1D model. This analysis should provide an understanding of PDI interactions on NSTX for HHFW, an ability to evaluate planned HHFW experiments for susceptibility to parasitic PDI losses, and approaches to minimizing these losses and optimizing the current drive efficiency.

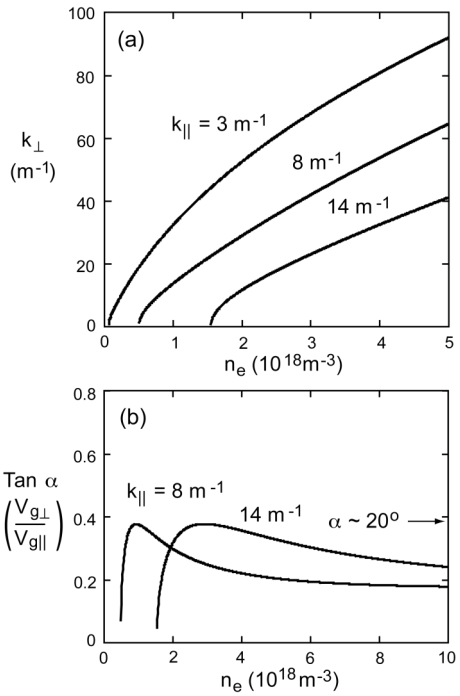

Figure. 4.2.1: High harmonic fast wave propagation characteristics for total magnetic field B = 2.82 kG at the antenna location on NSTX [toroidal field B_ϕ (R_o) = 4.5 kG, plasma current I_P = 0.6 MA]. (a) Perpendicular wavenumber $k_\perp$ versus density for parallel wavenumbers $k_{||}$ = 3 m^{-1}, 8 m^{-1} and 14 m^{-1}. (b) The tangent of the propagation angle α relative to the direction of B versus density. The onset density is $\propto B * k_{||}^2/\omega$ *and* $\alpha < 20^o$.

The HHFW research to date on NSTX has been focused on how to optimize coupling of the HHFW power to the core plasma. It became clear in 2005 that heating for current drive phasing of the antenna (-90° between adjacent antenna element currents) was about ½ as efficient as for heating phasing (180°) [4.2.8]. The plasma dispersion relation pointed to the onset of perpendicular propagation of the fast waves close to the antenna/wall surface as being a possible

contributor to the enhanced surface loss at the lower phasing values (longer wavelength) as shown in Fig. 4.2.1(a). Indeed, increasing the magnetic field and lowering the edge density in 2006 resulted in a heating efficiency at -90° being equal to that at 180° [4.2.3]. Also, above onset the direction of the ray path in the HHFW regime is about 20° to the direction of the magnetic field, as opposed to the low harmonic case for which the angle increases with density into the plasma as shown in Fig. 4.2.1(b). This results in surface fast waves, especially for higher m modes, and for those waves entering the core of the plasma tends to keep the waves confined to the outer region of the plasma in major radius due to the up-shift in $k_{||}$ along the ray path. GENRAY analysis shows this effect for a single ray in Fig. 4.2.2 [4.2.9] and 3D AORSA modeling demonstrates this effect in the volume of the plasma in Fig. 4.2.3 [4.2.10].

The focus of the HHFW theory and modeling efforts during the five-year plan period will expand to

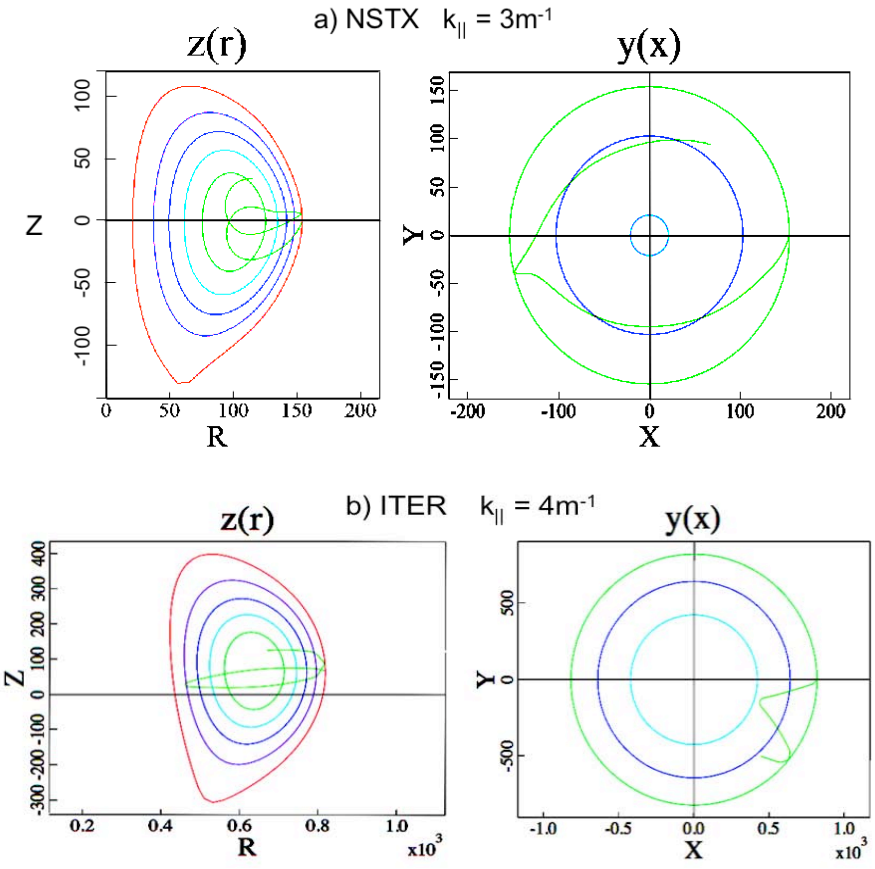

Figure 4.2.2: a) GENRAY modeling of ray path for NSTX conditions with $k_{||} = 3m^{-1}$. Note that the ray does not go through the plasma core. b) Similar modeling for ITER conditions with $k_{||} = 4m^{-1}$. Note that the ray propagates more radially and goes through the plasma core.

include other areas of importance including:

1. Mapping out propagation characteristics for L-Mode and H-mode plasmas:
   - Density versus magnetic field along the ray path can affect the path and hence the location of power deposition.
2. Understanding the fast wave damping mechanisms:
   - Core: Landau/Transit time magnetic pumping and short wavelength mode conversion effects.
   - Edge: Surface wave damping via collisions, sheaths, wall/antenna currents, and PDI heating.
3. Predicting conditions required to optimize plasma heating and current drive (CD):
   - Co vs counter CD
   - Can HHFW CD be used to help stabilize core MHD, e.g., by increasing reverse shear in the core with counter CD?

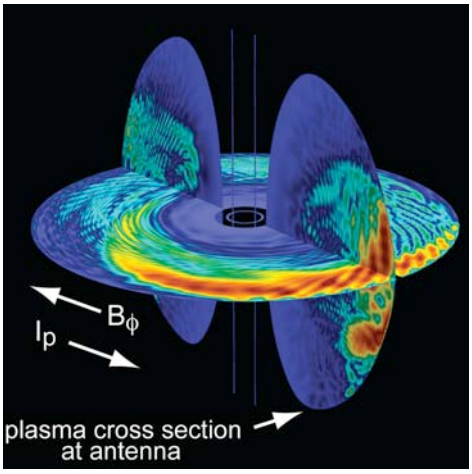

Figure 4.2.3: 3-D AORSA modeling shows propagation to be near the wall and primarily outside the major radius on NSTX (-90° case, summed over 81 toroidal modes). The antenna is located on the right hand side of the figure.

4.2.3 HHFW Heating System

The present HHFW system on NSTX [4.2.11] has 12 adjacent antenna straps which cover ~ 90° of the torus toroidally as shown in

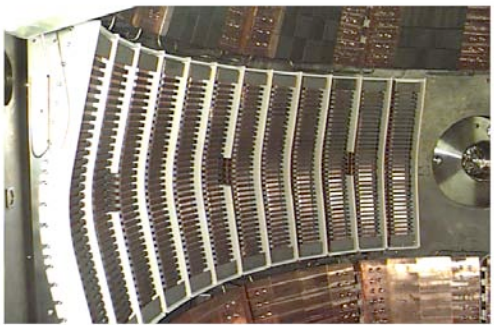

Figure 4.2.4: NSTX HHFW antenna

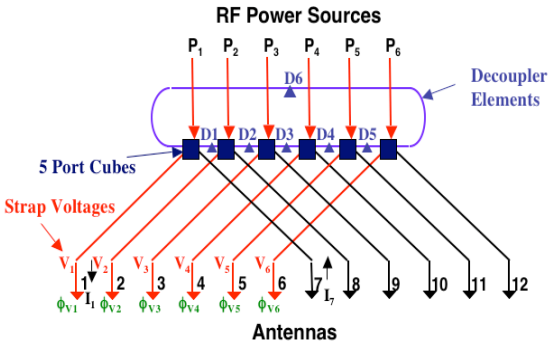

Figure 4.2.5: HHFW Antenna feed system

Fig. 4.2.4. Pairs of the straps are powered with six sources via a transmission/impedance matching system comprised of 6 long transmission lines, 6 phase shifters, 6 stubs, and 6 decoupling loops (Fig. 4.2.5). The system uses digital control of power and phase, and automated matching calculations to facilitate rapid changes in matching for desired phases. To meet the need for more HHFW power with a larger antenna-plasma gap to help avoid bombardment of the antenna, especially for H-mode operation at full beam power, a series of HHFW system upgrades are planned:

2008-09:

A major upgrade of the antenna will consist of providing two feedthroughs per antenna strap, as shown in Fig. 4.2.6. This should permit a threefold increase in power capability for the present antenna at the same RF voltage.

2010:

The HHFW antenna will be upgraded for resilience to ELMs during H-mode with the addition of an ELM dump.

2011-13:

Further improvements to voltage standoff (to minimize the RF-induced electric field) will be made.

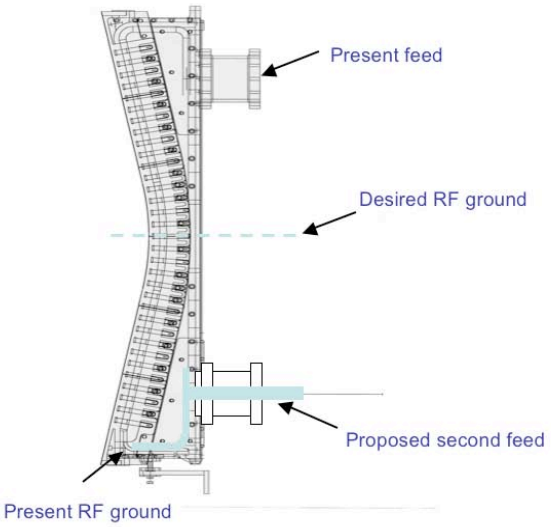

Figure 4.2.6: Planned HHFW antenna upgrade to two feedthroughs per strap

Diagnostics planned for HHFW Research:

In addition to the diagnostics needed to operate and protect the HHFW antenna array (such as acoustic arc detectors in the pressurized transmission lines), information on the RF interaction with both the edge and the core plasma is needed to improve the HHFW performance and reliability. To make progress in modeling development, the codes need both accurate input parameters for their analyses and detailed measurements for output validation.

A wide array of edge diagnostics is presently employed in the study of power coupling/propagation and more will be deployed in the future. A fast ion gauge located behind the array is used to monitor the local neutral pressure. It is observed that the pressure increases with both RF power and with decreasing wavelength; this high neutral pressure can lead to increased collisional damping and breakdown in the

antenna. The heating of edge ions is measured with the Edge Rotation Diagnostic, which shows increased heating of edge ions as the wavelength is increased. Langmuir probes positioned between antenna boxes, in the shadow of the local limiter, have seen increases in the local plasma potential with decreasing wavelength. The characteristic spectrum of PDI, postulated as the mechanism for edge ion heating, is observed with both a Langmuir probe and a microwave reflectometer. B-dot probes that measure the RF fields near the wall have seen increased signal strength when plasma conditions and antenna phasing are expected to support surface wave propagation. A visible light camera looking at the Faraday shield has been able to identify hot spot formation as a precursor to some antenna arcs.

Light pipes will be added to the antenna enclosures during the opportunity presented by the HHFW antenna upgrade in 2008-9, giving the ability to look at impurity spectra and to identify internal arc locations. Additional B-dot probes will be added to study and to minimize the power loss associated with surface waves. The RF wave monitoring electronics in the edge density reflectometer will be upgraded for improved operation over a 2-50 MHz range, permitting observation of both the PDI daughter wave spectra (low frequency quasi-modes and higher frequency IBW modes). A dedicated IR camera could be used to study the plasma interaction with the front surface of the antenna.

HHFW power propagation and deposition in the core is inferred from traditional diagnostics such as Thomson scattering, soft x-ray arrays, and CHERS. Progress has been made in reducing the NBI perturbation on the plasma during RF operation, permitting MSE measurements to be made for HHFW current drive. More information is needed on the wave activity in the plasma core with regard to propagation and mode conversion. Direct observation of the RF wave structure in the core may be possible once the NSTX high-k scattering system is upgraded to detect 30 MHz frequencies in 2009. This capability is needed to make detailed comparisons to RF code predictions.

4.2.4 Status of HHFW Research

Significant progress in HHFW research has been made during the period covered by the previous five-year plan. In particular, efficient HHFW heating of L-mode plasmas was demonstrated in 2006-7 for heating and current drive antenna phasings, and demonstrated in 2007-8 in the presence of neutral beam heating. Also in 2007, analysis of MSE measurements of current drive has provided a quantitative

comparison to theoretical predictions of the current drive at RF power levels of ~ 2MW in L-mode plasmas. Optimization of heating and current drive at higher power should make very clear the appropriate conditions for applying HHFW to heat and drive current on NSTX and for applying HHFW to future ST devices.

HHFW Coupling Physics:

It has been demonstrated that keeping the edge density near the antenna low relative to the onset density

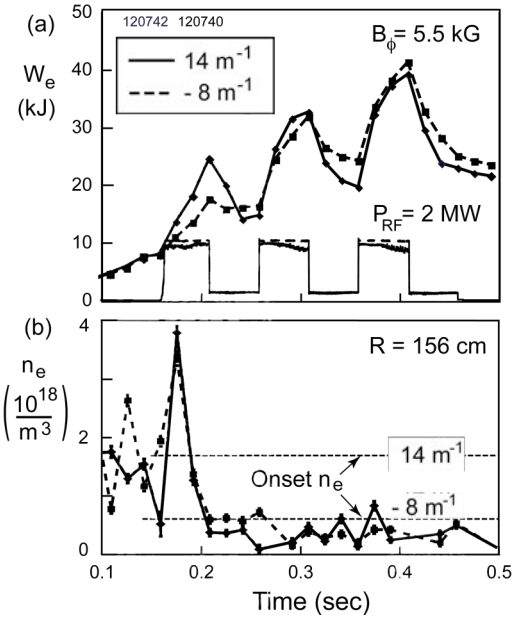

Figure 4.2.7: a) Time dependence of electron stored energy (W_e) with maximum modulated RF power of 2 MW, one with $k_{||}$= 14 m^{-1} (solid curve) and the other with $k_{||}$ = -8 m^{-1} (dashed curve). (b) Edge electron density (2 cm in front of Faraday shield) versus time. The onset density for $k_{||}$= 14 m^{-1} and $k_{||}$= -8 m^{-1} perpendicular propagation indicated by horizontal dashed lines.

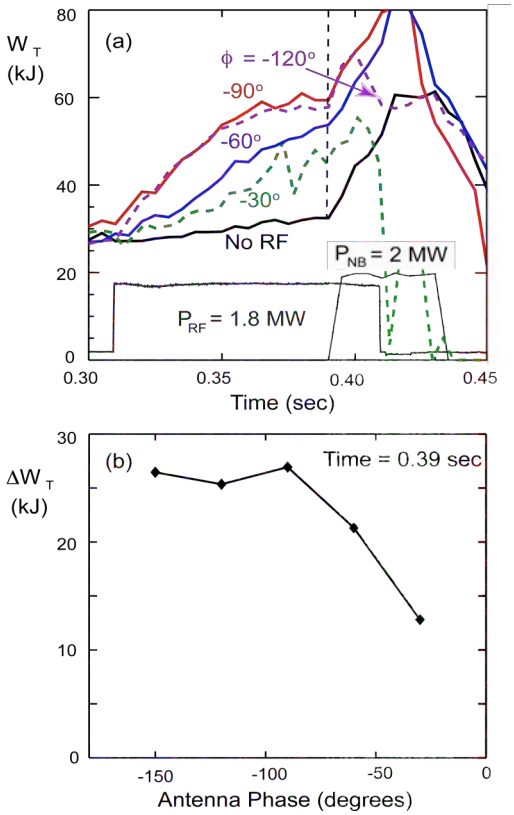

Figure 4.2.8: (a) Time dependence of total stored energy (W_T) P_{RF} = 1.8 MW versus phase ϕ between antenna straps (b) Change in total stored energy (ΔW_T) at time = 0.39 s showing the falloff of heating at longer wavelengths, $|\phi| < 90^o$. (B_ϕ = 5.5 kG, I_p = 0.6 MA,

for perpendicular propagation ($\propto B \times k_{||}^2/\omega$) results in a substantial increase in coupling efficiency for current drive phasing $k_{||} \approx$ -8 m^{-1} (-90^o) [4.2.3, 4.2.4]. This is demonstrated in Fig. 4.2.7 where it is shown that the efficiency at $k_{||} \approx$ -8 m^{-1} is equal to that for $k_{||} \approx$ 14 m^{-1} (180^o) for the last two RF power pulses, when the density is at or below the onset

density 2 cm in front of the antenna. However, the efficiency for $k_{||} \approx -8$ m^{-1} during the first RF power pulse is half the $k_{||} \approx 14$ m^{-1} value where the density is ~ 3 × the onset value for $k_{||} \approx -8$ m^{-1}.

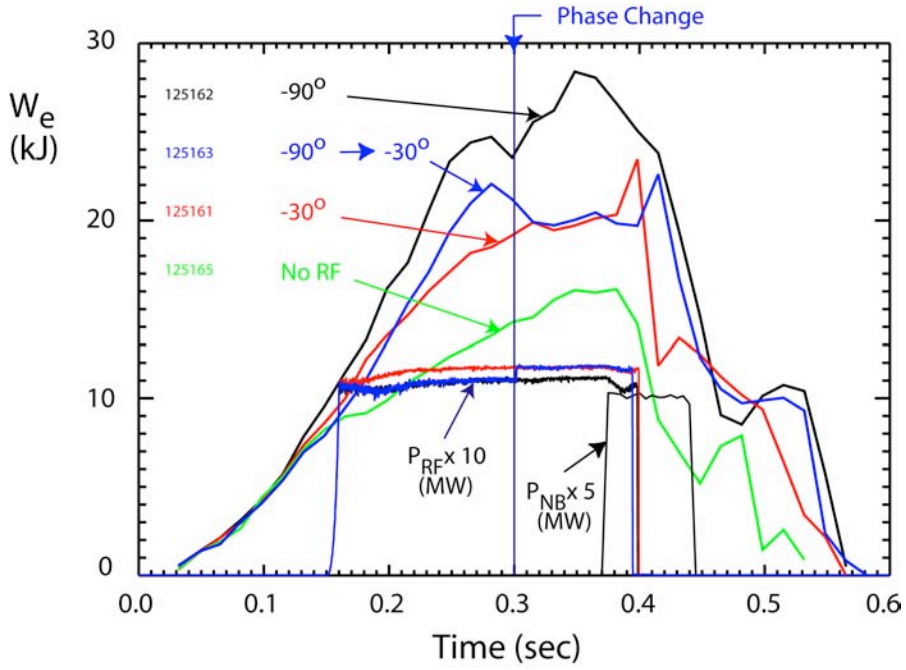

Figure 4.2.9: HHFW Heating at - 30° is ~ 1/2 that at - 90°

The fact that the placement of the perpendicular propagation onset is an important condition for determining surface wave losses is further illustrated in Fig. 4.2.8, where it is shown that at even longer wavelengths (lower $k_{||}$ or phase) the stored energy falls off with phase. Note that the onset density is proportional to $k_{||}^2$ and is pushed against the antenna/wall at the lower phases. Also, whereas the wavelength plays a dominant role in RF surface losses, the data of Fig. 4.2.8 suggests that the cancellation of reactive currents from near strap currents is not as important.

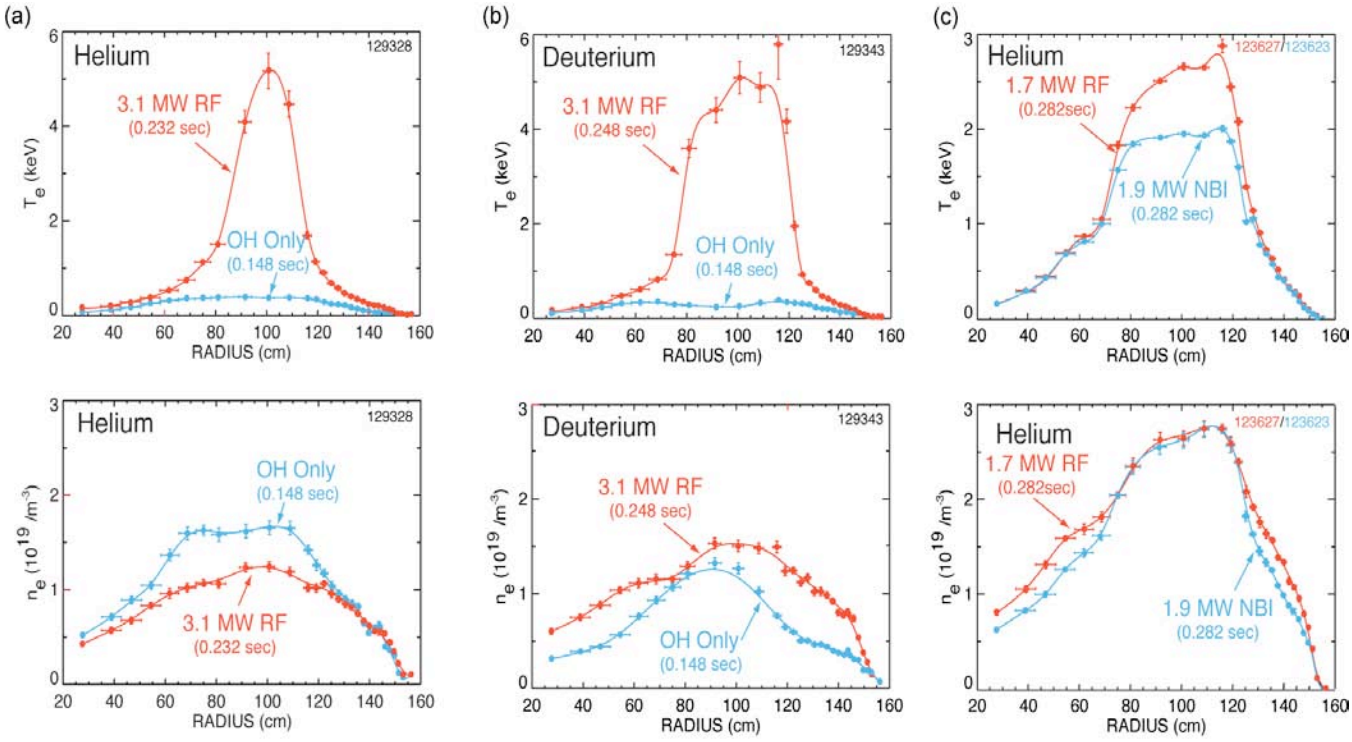

Figure. 4.2.10: T_e and n_e profiles for high $T_e(0)$ plasma heated with 3.1 MW of HHFW power coupled into (a) helium and (b) deuterium discharges with $B_t(0) = 0.55$ T. c) Significant electron heating observed in the core of $B_t(0) = 0.55$ T helium discharge when 1.7 MW of HHFW power is added to 1.9 MW of NBI power.

To further demonstrate the surface losses associated with having the onset density above the edge density at the antenna/wall, the core heating has been measured for a relatively long RF pulse during which the phase was changed from -90^o to -30^o. The results are compared to cases without the phase change and to the no RF case in Fig. 4.2.9. Again, this data shows that the wavelength plays a dominant role in RF surface losses and that these losses do not appear to be dependant on core damping (the increase in central temperature during the -90^o period did not result in better heating during the -30^o period).

Significant HHFW electron heating has been obtained with current drive phasing for L-mode helium and deuterium discharges with HHFW alone (Fig 4.2.10(a) and (b)) and in conjunction with neutral beam heating (Fig 4.2.10(c)). Promising results have also been obtained for HHFW coupling into low plasma current (I_p < 250 kA) H-mode plasmas where bootstrap current fractions up to 85% have been generated

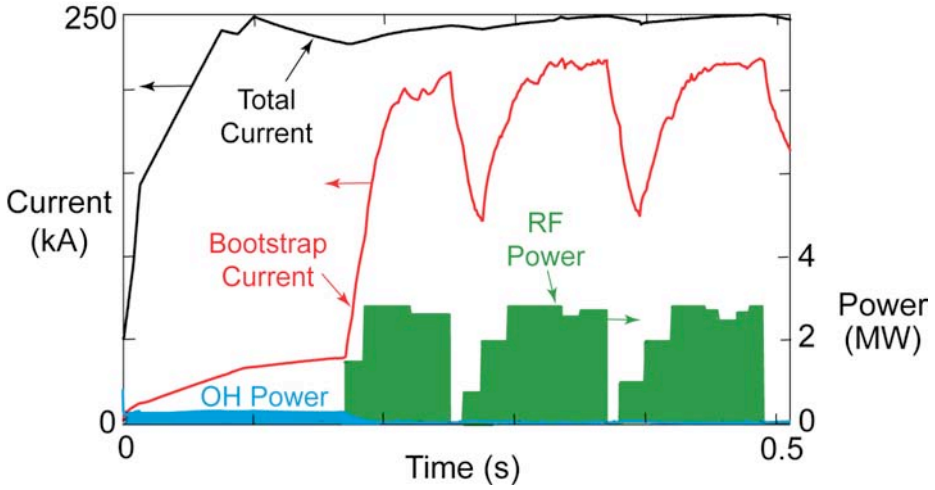

Figure 4.2.11: HHFW heating in low plasma current H-mode plasma generates 85% bootstrap fraction.

(Fig. 4.2.11). This result supports the use of HHFW for plasma current overdrive using bootstrap and HHFW current drive as a tool for ramping plasma current to I_p ~ 500 kA, a level sufficient for effective NBI heating.

Initial motional Stark effect (MSE) measurements of the current profile in helium L-mode discharges (Fig. 4.2.12) show clear evidence of core HHFW current drive with -90° phasing. The MSE RF-driven current profile measurements are consistent

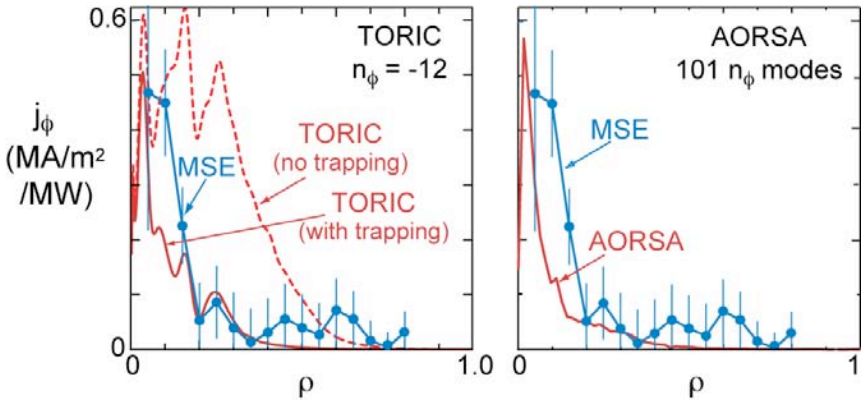

Figure. 4.2.12: Measurement and simulations of rf-driven CD for -90° phasing

with predictions from AORSA and TORIC full wave simulations, although the predicted profiles are narrower, perhaps because the simulations do not include radial transport.

4.2.5 HHFW Research Plan for 2009-2013

The HHFW research in 2009-10 will be directed toward extending the coupling and current drive studies to deuterium H-mode conditions. These experiments will be enabled by improvements in the HHFW antenna, including the double feed upgrade in 2008-9 and the ELM resilience system in 2009-10. In addition there will be some experiments in 2009-10 to couple HHFW into low temperature, low plasma current discharges to support the development of HHFW-assisted plasma ramp-up scenarios.

2009-10:

- Optimize heating and current drive operation with NBI for L-mode and H-mode with the upgraded antenna and using guidance of modeling.
- Use larger plasma-antenna gap permitting greater stability and at higher power (more voltage standoff and greater power for same voltage). Also, faster feedback control of the plasma position would help to reduce the beam interaction with the antenna. An even larger gap will probably be required for operation with all three high-power NBI sources in the H-mode regime.
- HHFW-assisted startup/ramp-up plasmas using low T_e, I_p ohmic plasmas

2011:

- Optimize heating and current drive operation with NBI deuterium H-mode with fully upgraded HHFW antenna and lithium conditioning.
- Benchmark core current drive against advanced RF codes.
- Optimize HHFW-assisted ramp-up plasmas using low T_e, I_p ohmic plasmas.
- Combine HHFW coupling into plasma ramp-up and 28 GHz ECH-assisted non-inductive startup.

2012-13:

- Support very long pulse plasma scenario; integrate HHFW controls into NSTX PCS, control q on-axis and develop very long pulse, high power operation at toroidal fields up to 1 T.
- Support fully non-inductive startup and ramp-up, combining 28 GHz ECH-assisted CHI or PF-only startup and HHFW-assisted ramp-up.

4.3 Electron Cyclotron and Bernstein Wave Physics

4.3.1 ECW/EBW Research Goals

Off-axis radiofrequency-driven current is expected to be critical for stabilizing solenoid-free ST plasmas when β > 20% [4.3.1]. For example, modeling predicts that adding 1 MA of off-axis EBW current drive (EBWCD) to the ST-CTF [4.3.2] would significantly improve the performance of the plasma (Fig. 4.3.1). The long-term research goal for the EBW research program on NSTX is to assess the viability of EBWCD as a tool for generating this critical stabilizing current. There are several intermediate research goals for the 2009-2013 research program that support solenoid-free ST research, they are:

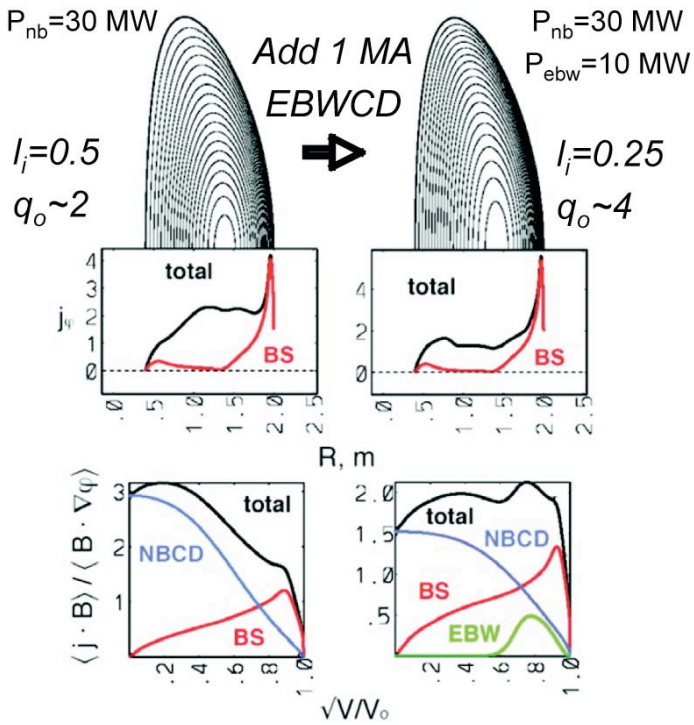

Figure 4.2.1: Adding 1 MA of off-axis EBWCD to CTF plasma generating wall loading of 1 MW/m^2 can decrease l_i from 0.5 to 0.25 & increase q_o from ~ 2 to ~ 4. As a result, the β_n limit increases from 4.1 to 6.1 and the β_t limit increases from 19% to 45%.

1. Continue to optimize EBW coupling in H-mode through the use of EBW emission radiometry and a combination of lithium injection and the Liquid Lithium Divertor (2009-10)
2. Develop ECH-assisted plasma startup with 350 kW of 28 GHz power in order to increase T_e sufficiently for effective HHFW coupling (2011).
3. With additional incremental funding, study EBW coupling with up to 700 kW of 28 GHz power (2012-13).

If an EBW heating system is not installed on NSTX it may be possible to continue this research through collaboration on MAST where a 350 kW 28 GHz gyrotron is being installed this year in collaboration with Oak Ridge National Laboratory.

4.3.2 EBW Physics

When $\omega_{pe} > 1.6\ \omega_{ce}$, where ω_{pe} is the electron plasma frequency and ω_{ce} is the electron cyclotron frequency, the electrostatic EBW [4.3.3] can propagate across the magnetic field. This regime is normally referred to as the overdense regime, and it is a regime that is not accessible to conventional ECH or ECCD. Except during plasma start-up and the initial stages of plasma current ramp-up, NSTX discharges operate well inside this overdense regime. EBWs are strongly absorbed at electron cyclotron resonances and have the potential to provide local electron heating (EBWH) and EBWCD. However, EBWs can only propagate inside the upper hybrid resonance (UHR) that surrounds overdense plasma, so EBWH and EBWCD systems that have microwave launchers external to the plasma, must employ a mode conversion process in the vicinity of the UHR to couple the microwave power to the EBWs. Electromagnetic radiation can couple to EBWs either by tunneling from the extraordinary mode to the EBW (X-B conversion) [4.3.4] or by mode conversion from the ordinary mode, via the slow extraordinary mode, to the EBW (O-X-B conversion) [4.3.5]. For X-B conversion X-mode polarized microwave power is launched normal to the magnetic field (Fig. 4.3.2(a)). The left hand cutoff of the slow X-mode (SX), the UHR, and the right hand cutoff of the fast X-mode (FX) form a cutoff-resonance-cutoff triplet allowing the fast X-mode electromagnetic wave to tunnel through the UHR to the slow X-mode [4.3.4]. For O-X-B conversion (Fig. 4.3.2(b)) elliptically polarized microwave power is launched at an oblique angle to the magnetic field that is chosen to make the X-mode and O-mode cutoffs coincident [4.3.6, 4.3.7].

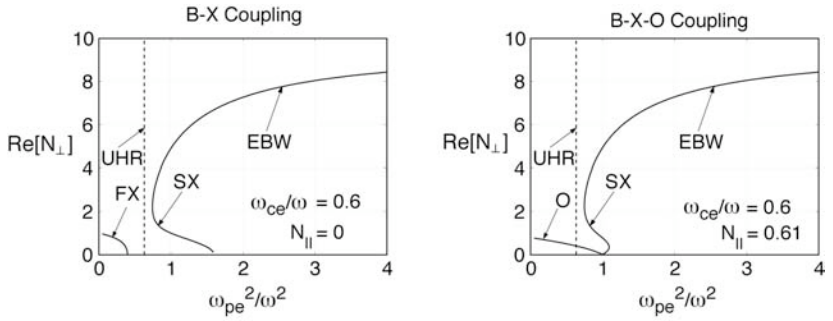

Figure 4.2.2: EBW and electron cyclotron wave roots of the real part of $N_\perp$ as a function ω_{pe}^2/ω^2 for two EBW coupling schemes have been studied on NSTX and other machines: (a) perpendicular ($N_{//} = 0$) X-B coupling where the fast X-mode (FX) tunnels to the slow X-mode (SX) and (b) oblique O-X-B coupling, where $N_{//} = N_{//,opt} = 0.61$.

EBWs can exhibit large changes in refractive index after being launched. The change in the parallel

refractive index, $N_{//}$, is given by:

$$N_{//} \propto -\frac{1}{(k_\perp \rho_e)^2}\left|\frac{B_\theta}{B}\right| n_\perp \sin\theta\left(\frac{\Delta r}{R}\right),$$

where $ck_\perp/\omega = N_\perp$, c is the speed of light, ω is the wave angular frequency, ρ_e is the electron Larmor radius, B_θ is the poloidal component of the magnetic field, $|B|$ is the magnitude of the total magnetic field, θ is the poloidal angle measured from the outboard side of the plasma midplane, Δr is the radial distance of propagation of the ray, and R is the major radius. For $\theta \sim 0$ the shift in $N_{//}$ is minimal. However, for EBWs launched above or below the plasma midplane the change in $N_{//}$ can be large, since in the outboard edge region of the ST plasma the poloidal and toroidal magnetic field strengths are comparable. EBWs heat electrons and drive current at the Døppler shifted cyclotron resonance, given by:

$$\gamma\omega = k_{//}\frac{p_{//}}{m_e} + n\omega_{ce},$$

where γ is the Lorentz relativistic factor, $p_{//}$ is the parallel momentum, m_e is the electron rest mass, and n is the harmonic number of the electron cyclotron resonance. So the location where electron heating and current drive occurs depends sensitively on $N_{//}(= ck_{//}/\omega)$, and therefore on where the EBW coupling occurs relative to the plasma midplane. Also, the direction of the driven current depends on whether the EBWs are launched above or below the midplane [4.3.8]. Current drive occurs via two mechanisms; *Fisch-Boozer* current drive [4.3.9], where EBWs predominantly heat electrons with one sign of $v_{||}$, creating an asymmetric resistivity, and *Ohkawa* current drive [4.3.10], where EBWs increase the $v_\perp$ of passing electrons in one direction so that they become trapped, resulting in a net current being driven in the opposite direction. Normally in an ST both these current drive mechanisms are present, driving current in opposite directions. Fisch-Boozer current drive dominates near the magnetic axis and Ohkawa current drive dominates off-axis on the low field side, where there is a large trapped electron population in an ST.

4.3.3 28GHz ECH/EBWH System

A 28 GHz ECH system will be installed on NSTX in 2011 [Fig. 4.3.3]. This system will use a gyrotron with an output power of up to 350 kW. For the 2011 campaign, this system would employ a fixed horn antenna on the plasma midplane to launch X-mode microwave power to support second harmonic ECH-assisted plasma startup experiments at $B_t(0) = 0.5$ T and fundamental O-mode ECH at $B_t(0) = 1$ T. Unless

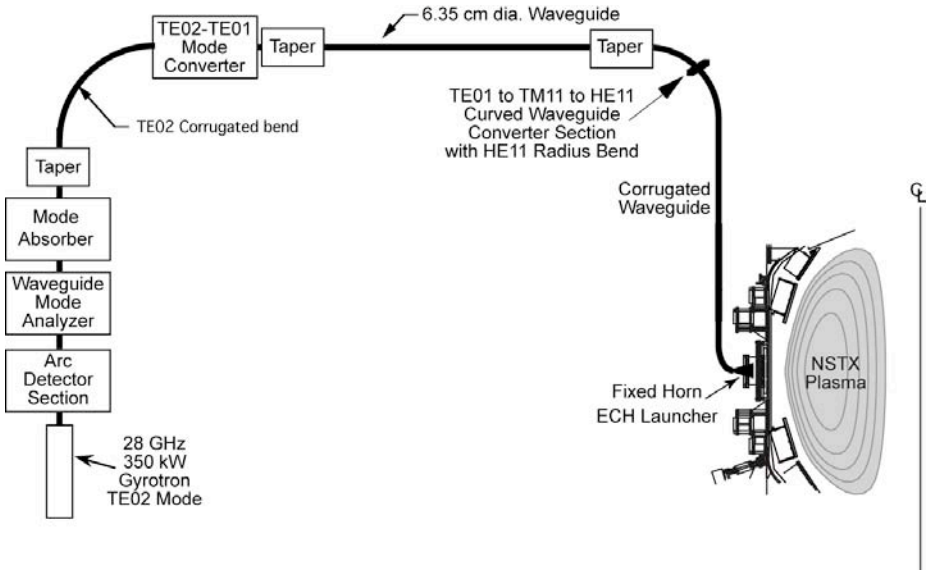

Figure 4.2.3: 350 kW, 28 GHz, 500 ms heating system proposed for installation on NSTX in 2011. With additional incremental funding the system would be upgraded to 700 kW in 2012.

incremental With incremental funding a second 350 kW 28 GHz gyrotron is proposed for 2012, increasing the total available RF power to 700 kW. With the installation of the new center-stack on NSTX in 2012 operation at 1 T will allow fundamental frequency 28 GHz EBWH which has significantly better radial access than second harmonic EBWH. MAST is planning to install a 350 kW 28 GHz ECH/EBWH system by the end of 2008, so if the proposed 28 GHz NSTX EBW heating system is not installed by 2012 it may be possible to conduct some of the proposed 28 GHz EBW research on MAST by upgrading their system.

4.3.4 Status of EBW Research

This section summarizes significant advances in EBW research on NSTX and other devices since the last NSTX 5-year research plan in 2003. High levels of EBW coupling efficiency have been measured via

thermal EBW emission from the magnetic axis of NSTX and Fokker-Planck modeling of NSTX discharges has predicted that efficient off-axis Ohkawa current drive is achievable in $\beta > 20\%$ plasmas. There have also been recent encouraging experimental results on MAST and TCV that show clear indications of O-X-B EBW heating, and recently efficient EBW heating of PF-only startup discharges in MAST has been measured at 28 GHz.

Status of NSTX Experimental EBW Research:

Except for power dependent effects like PDI, the O-X-B mode conversion process involved in coupling microwaves to EBWs for EBWH and EBWCD is the reciprocal of the B-X-O mode conversion mechanism involved in coupling thermal EBW emission out of the plasma. So it is possible to study EBW coupling efficiency by measuring thermal EBW emission [4.3.11]. Initial B-X-O coupling studies on NSTX were performed in 2004 with a dual-channel, 8-18 GHz radiometer connected to a fixed, obliquely-viewing, quad-ridged antenna with its ridges aligned to simultaneously measure the radiation temperature of EBE polarized parallel ($T_{//}$) and perpendicular ($T_{\perp}$) to the magnetic field at the upper hybrid resonance (UHR) [4.3.12]. An example of data from this antenna is shown in Fig. 4.3.4, which shows the evolution of the EBW radiation temperature, $T_{rad} = (T_{//}+T_{\perp})$, for a L-mode plasma with $B_T(0) = 4$ kG and a flattop current. $I_p = 800$ kA between 0.27 and 0.46 s. The EBW coupling efficiency, T_{rad}/T_e, where T_e is the electron temperature of the EBW emitting layer, was measured to be 80 ± 20% at 16.5 GHz, in good agreement with the ~ 65% EBW coupling efficiency predicted by a model that includes a 1-D full wave calculation of the EBW mode conversion at the UHR, radiometer antenna pattern modeling and 3-D EBW ray tracing and deposition modeling [4.3.13]. Emission at 16.5 GHz was from the fundamental electron cyclotron

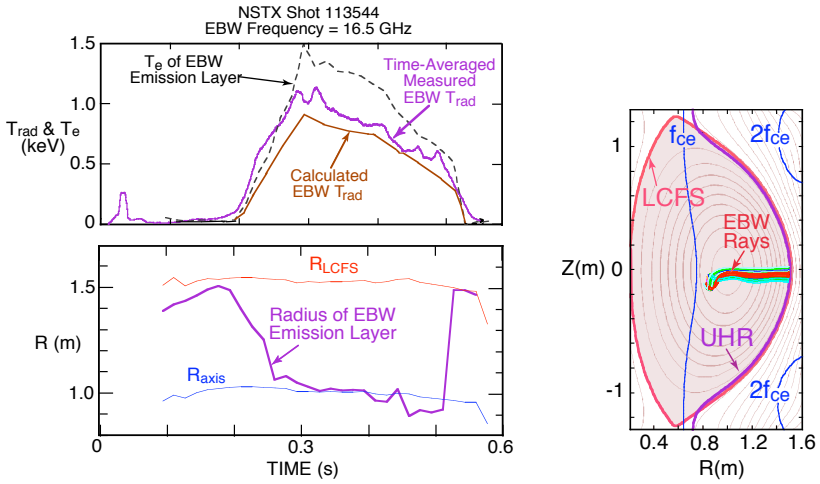

Figure 4.3.4: 80% f_{ce} B-X-O coupling measured in NSTX L-mode edge plasmas, consistent with modeling

resonance at the plasma magnetic axis during the I_p flattop. The measured EBE polarization ratio, $T_{//}/T_{\perp}$, was also measured to be in reasonable good agreement with theoretical modeling.

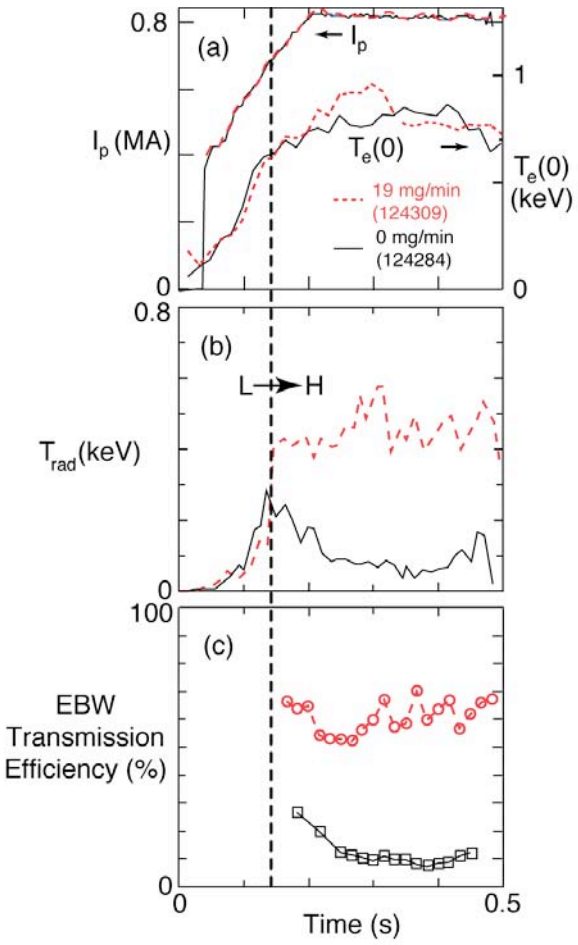

Figure 4.3.5: (a) Plasma current and central electron temperature evolution for two H-mode plasmas, one without lithium conditioning (black solid line) and one with lithium conditioning (red dashed line). (b) Time evolution of EBW radiation temperature for fundamental emission from the plasma core at 18 GHz and (c) EBW transmission efficiency from the core to the EBW radiometer antenna.

In 2005 a pair of remotely steered B-X-O antennas were installed on NSTX [4.3.14], allowing the B-X-O emission process to be studied in more detail. Results showed that the EBW coupling efficiency peaks at a poloidal and toroidal angle that is close to the direction predicted by theory [4.3.15]. Recent studies of B-X-O emission from H-mode plasmas in NSTX show a wide range of behavior; sometimes the coupling efficiency remains relatively high (~ 50%) throughout the H-mode phase, sometimes it gradually decays, and sometimes the coupling efficiency collapses soon after the L to H transition. Measurements and modeling of EBW emission on NSTX are supportive of collsional damping of the EBW, prior to mode conversion, as being a possible major cause for the degradation of EBW emission in H-modes. Collisional damping is expected to become important when T_e near the EBW mode conversion layer is < 20 eV. In NSTX H-mode plasmas, measured T_e in the B-X-O mode conversion region, particularly for f_{ce} emission, can be as low as 10 eV. During NSTX experiments in 2007 there was strong evidence that Li conditioning can significantly enhance B-X-O emission from H-modes, either by changing the density scale length or increasing T_e in the conversion region [Fig. 4.3.5]. It is possible that EBW collisional damping may not be a problem for EBW heating of H-modes if the incident microwave power

can heat the EBW mode conversion region sufficiently to avoid EBW collisional loss.

Status of Experimental EBW Research on Other Devices:

Following the first demonstration of O-X-B EBWH in the W7-AS stellarator in 1997 [4.3.16] there have been several O-X-B heating experiments on other devices that show encouraging results. 60 GHz B-X-O EBW heating experiments conducted on the MAST ST used three plasma scenarios [4.3.17].

MAST was the first ST device to use O-X-B heating. The O-X-B coupling efficiency was at least 50% in high-density ELM-free H-mode discharges. In sawtoothing H-mode plasmas, a 10% increase of stored energy was measured during EBWH, and a 10% increase in T_e was measured in small ohmic H-mode plasmas [Fig 4.3.6]. Future plans on MAST call for the installation of a 1 MW 18 GHz O-X-B EBWH system. Recently, there have also been plasma startup experiments on MAST that employ a 28 GHz heating system. 90 kW of RF power generated 32 kA of plasma current, without using the central solenoid, in good agreement with modeling [4.3.18]. The resulting plasma had a $T_e \sim 500$ eV and $n_e \sim 10^{18}$ m^{-3}. This result suggests the NSTX 350 kW, 28 GHz ECH system, that will be operational in 2011, should be able to heat the plasma sufficiently to allow effective HHFW heating.

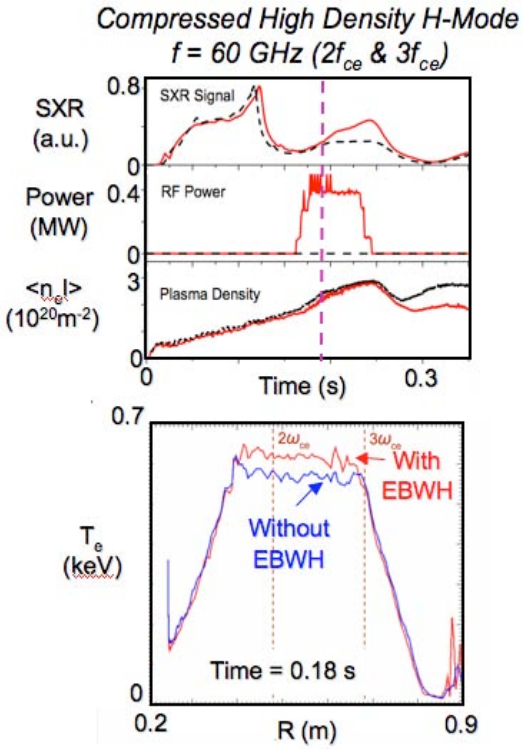

Figure 4.3.6: 60 GHz EBW heating via O-X-B coupling demonstrated on MAST.

The first demonstration of EBWH via O-X-B mode conversion in an overdense conventional aspect-ratio tokamak was achieved in the TCV device [4.3.19]. The central electron temperature evolution during 82.7 GHz EBWH was measured to increase by 80 eV when the RF power was increased from 1 to 2 MW [Fig. 4.3.7].

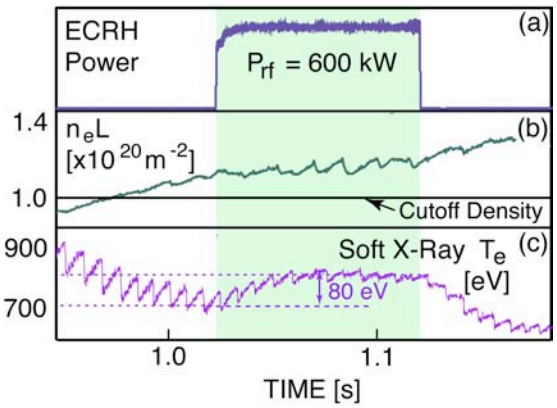

Figure 4.3.7: EBW heating via O-X-B coupling demonstrated on TCV. (a) 600 kW of 82.7 GHz power was coupled into (b) an overdense TCV plasma via O-X-B coupling.(c) At 60% of the RF power was absorbed by the plasma at r/a ~ 0.65, increasing T_e, as measured by soft X-rays, by 80 eV.

The optimum injection angle for O-X-B conversion was obtained experimentally by measuring the reflected microwave radiation during a two-dimensional angle scan. Ray tracing simulations yielded an optimum launch angle that was in good agreement with the measured angle. About 60% of the RF power was absorbed after conversion to EBWs.

Status of EBW Theory and Numerical Modeling:

The GENRAY numerical ray tracing code [4.3.8, 4.3.20] and the CQL3D Fokker-Planck code [4.3.21] have been used to model EBW propagation, heating and current drive in NSTX discharges with $\beta \geq 20\%$. Efficient off-axis Ohkawa

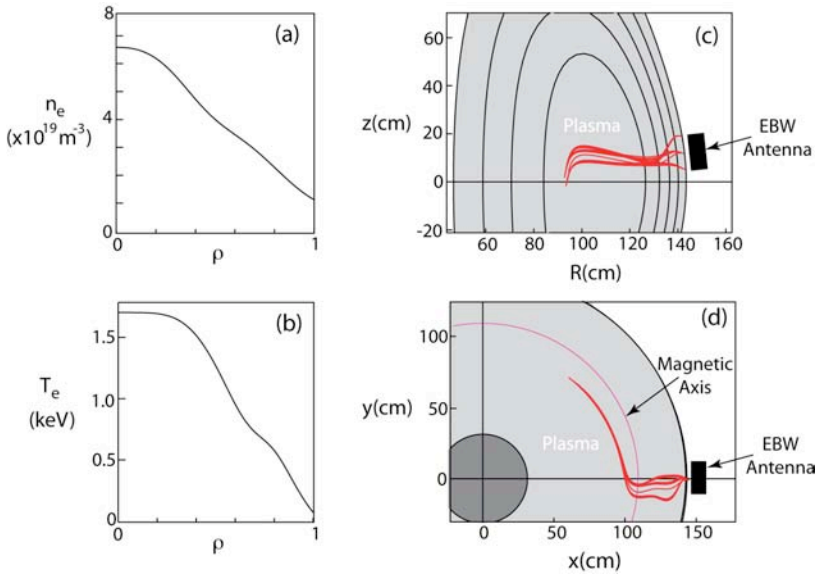

Figure 4.3.8: (a) n_e and (b) T_e profiles used to model 28 GHz EBW propagation and damping in a $\beta = 20\%$, $B_t(0) = 0.55$ T NSTX plasma. (c) Poloidal and (d) toroidal midplane projection of EBW rays calculated by GENRAY for a launched spectrum with $N_{//} = -0.55 \pm 0.05$. 28 GHz EBW power is absorbed near the magnetic axis.

current drive at a normalized minor radius, $\rho \sim 0.7$, and on-axis Fisch-Boozer current drive is predicted

[4.3.22] for a range of plasma and EBW launch scenarios. An example of 28 GHz EBW ray tracing results from the GENRAY for a $\beta = 20\%$ NSTX plasma with a vacuum toroidal field, $B_t(0) = 0.55$ T is shown in Fig. 4.3.8. EBW power is deposited near the magnetic axis. Figure 4.3.9 shows the EBW power deposition and EBW-driven current profile calculated by the CQL3. 85% of the EBW power is absorbed by at the Doppler-shifted $2f_{ce}$ resonance, near $\rho = 0.2$, the remainder is absorbed at the Doppler-shifted $3f_{ce}$ resonance, also near the axis. The total EBW-driven current, generated in this case via the Fisch-Boozer current drive mechanism is 29 kA, corresponding to a current drive efficiency of 39 kA/MW. Synergy between EBWCD and the current driven by the electron bootstrap effect has been calculated to be relatively weak, typically <10%. However, the local bootstrap current density increases in proportion to increased plasma pressure, and this effect can significantly modify the radial profile of the RF-driven current density [4.3.23]. Benchmarking between GENRAY/CQL3D and the European code BANDIT-3D [4.3.24] for a NSTX EBWCD case shows good agreement for the magnitude, direction and location of the EBW-driven current. A recent reviews of the most important theoretical and numerical modeling results for EBWs in ST's can be found in references 4.3.25 and 4.3.26.

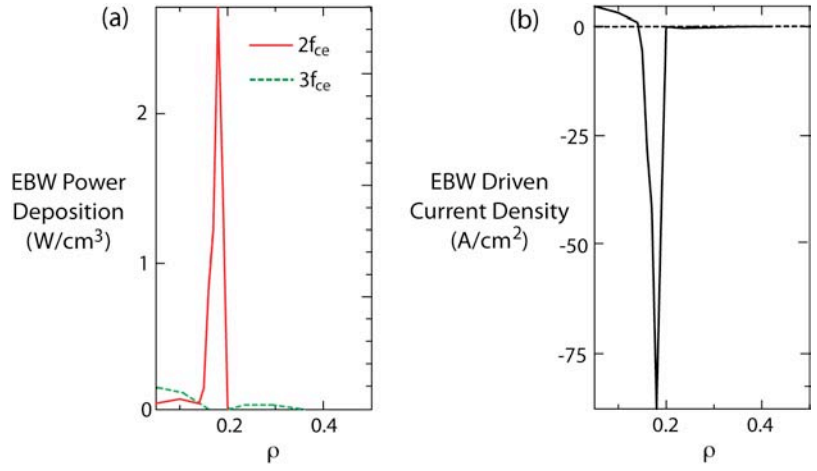

Figure 4.3.9 (a) EBW power deposition to electrons calculated by CQL3D for 750 kW of EBW power coupled into the plasma shown in Fig. 4.2.8. (b) EBW-driven current density calculated by CQL3D.

4.3.5 ECW/EBW Research Plan for 2009-2013

2009-10:

EBW studies during this period will focus on emission from low-density plasmas that will use lithium injection and the Liquid Lithium Divertor to keep the EBW mode conversion layer inside the separatrix to

avoid EBW collisional damping and mode conversion efficiency fluctuations due to scrape off density turbulence.

2011:

A 350 kW, 28 GHz gyrotron will be installed on NSTX. This system will initially be used for second harmonic X-mode ECH to heat CHI and PF-only startup plasmas and increase the electron temperature sufficiently to allow efficient HHFW heating. A fixed horn antenna will be used for these ECH-assisted plasma startup experiments. Experiments will explore the transition from ECH-assisted startup to HHFW-assisted plasma current ramp up.

2012-13:

In 2012, with additional incremental funding, we propose to install a second 350 kW 28 GHz gyrotron on NSTX, bringing the total available 28 GHz source power to 700 kW. This upgraded ECH system would initially be used for ECH-assisted plasma start-up research, but could also be used later for experiments to study EBW coupling physics via an oblique O-X-B launch. Based on emission studies in 2006-7 we can reasonably expect 70% EBW coupling efficiency, or about 500 kW of EBW power for 750 kW of 28 GHz source power. 28 GHz EBW experiments would greatly benefit from the higher toroidal field that will be generated using the new center-stack. Operation at a toroidal field of 1 T will allow fundamental frequency 28 GHz EBW heating where there is much better radial access compared to second harmonic heating. Results from these heating experiments could be used to benchmark EBW simulation codes. If the proposed 28 GHz EBW heating system is not installed on NSTX it may be possible to conduct some of this research program on MAST.

4.4 Energetic Particle Physics

4.4.1 Energetic Particle Research Goals

An important goal of the present proof-of-principle spherical tokamaks (ST) is to evaluate the role of fast ion driven instabilities in fast ion transport and confinement. The results will be used to validate linear numerical codes, such as NOVA/ORBIT and nonlinear codes such as M3D, which are used to predict the effect of fast-ion driven instabilities on fast ion transport. The codes may then be used with greater confidence to predict fast ion confinement in either an advanced ST such as NHTX/CTF/ARIES-ST or for tokamak reactors such as ITER and, ultimately, DEMO. Spherical tokamaks have relatively low toroidal field so the fast-ion Larmor radius is large compared to the plasma minor radius ($\rho_{fi} \approx 0.1 - 0.2\ a_p$) and the fast-ion velocity is much greater than the Alfvén speed ($V_{fi} \geq 2\ V_{Alfvén}$), and overlaps the expected fast ion (fusion-alpha) parameters for either tokamak reactors (ITER) or advanced STs. This regime of large Larmor radius and low Alfvén speed is a regime in which fast ion driven instabilities are potentially virulent. Considerable progress was made during the last five year period of operation on NSTX in identifying the broad spectrum of observed fast ion driven modes, as well as the drive and damping mechanisms. The redistribution or loss of fast ions will impact the interpretation of thermal transport data, beam driven currents and momentum transport, as well as having a potentially direct impact on the design of plasma-facing components in a reactor (due to the potential for localized heating or ablation from lost fast-ions). Recently added diagnostics, as well as diagnostics planned for the near future, will allow for more detailed studies of the saturation amplitude, internal structure, and the effects on fast ion transport. The higher field and second beamline will extend the range of fast ion parameters, expanding the parameter range of the data to be used for code validation.

Good experimental measurements are required to validate the codes developed to predict the effect of fast-ion driven instabilities on transport of fast ions. It is not only necessary to have good measurements of the equilibrium parameters, but the stability thresholds and saturation amplitudes of the fast ion modes must also be measured. The impact of these modes on the fast ion distribution must be measured, as well. NSTX has accumulated a comprehensive suite of diagnostics for these studies. Redistribution of fast ions is now measured with the scanning Neutral Particle Analyzer (NPA), solid-state Neutral Particle Analyzer

(ssNPA) and the new Fast-Ion D-Alpha emission diagnostic. Losses of fast ions are detected with the scintillator Fast Lost Ion Probe (sFLIP), an array of Faraday cups for detecting lost fast-ions (iFLIP), as well as the fast neutron rate diagnostics. The planned addition of a neutron collimator diagnostic will complement these existing fast ion diagnostics by providing an additional measure of confined fast ion redistribution. The effect of loss or redistribution of fast ions on beam-driven currents, and interpretation of momentum and thermal transport can be documented with current profile evolution measurements based on Motional Stark Effect (MSE) diagnostic data (which is unique in providing q-profile measurements in fields as low as 3.5 kG), plasma rotation measurements with the toroidal and poloidal CHarge-Exchange-Recombination (CHERS) diagnostic and the complete complement of kinetic profile diagnostics.

Analysis of the data collected on fast ion instabilities is supported through an active theoretical program. The NOVA-k code calculates the linear eigenmode structure, as well as most of the damping and drive terms. While NOVA is a linear code, the saturated amplitudes of the individual modes will be directly measured and can be used to normalize the eigenfunctions calculated with NOVA. The resulting spectrum of eigenmodes, together with the unperturbed fast ion distribution calculated with the TRANSP code, is used as input to the ORBIT code. The ORBIT code follows the trajectories of many fast ions, in the presence of modes, and can predict the resulting loss or redistribution of fast ions. A fully non-linear code, M3D, is used to self-consistently predict saturated mode amplitudes and fast-ion transport for comparison with the measured values. M3D is a "δf" code, where only the perturbed component of the fast ion distribution receives full kinetic treatment.

The presence of weakly damped plasma modes below the cyclotron frequency, revealed through excitation by beam fast ions, has suggested a unique heating method for spherical tokamaks. Although this method is different from the originally suggested alpha channeling [4.4.1] it serves the same goal of tokamak optimization by increasing its output power via minimizing electron heating and directing either auxiliary or fast ion produced power to heat thermal ions. A large amplitude wave at a fraction of the ion cyclotron frequency can stochastically heat thermal ions. The presence of weakly damped plasma modes in this frequency range suggests that excitation of these modes, with a driven antenna, to a sufficient amplitude would stochastically heat the thermal ions. The fundamental principles of stochastic heating

were developed in the late 1970's and early 1980's [4.4.2-4.4.6], and experiments validating the concept were done from the late 1980's to mid 1990's [4.4.7-4.4.11]. In the coming five years it is proposed to explore the possibility of using such a stochastic ion heating system on NSTX.

4.4.2 Energetic Particle Physics

The transport of fast ions can be greatly enhanced in the presence of multiple modes. This can mean either multiple modes of a similar type, for example several Toroidal Alfvén Eigenmodes (TAE), or, potentially, modes as disparate from TAE as Compressional Alfvén Eigenmodes (CAE) or fishbones. As the diffusive "step size" from interaction with fast ion instabilities tends to be proportional to the ion gyro-radius, fast ion losses in large, high field devices such as ITER are expected to be through the interaction of multiple modes [4.4.12]. The study of such multimode interactions will be a high priority in the next five years on NSTX. Strongly enhanced transport has been seen when multiple TAE modes interact, a process known as TAE avalanches [4.4.13-4.4.17]. Three-wave coupling of TAE, fishbones (kinks) and higher frequency Alfvén eigenmodes has also been seen [4.4.18], with some data suggesting that these modes may also interact through perturbations of the fast ion distribution.

The impact of these studies on future devices such as NHTX or ITER will be primarily through the numerical simulation code improvements needed to accurately model the NSTX data. The capability to predict stability thresholds for fast-ion driven instabilities in future fusion reactors is an important component of the design and identification of attractive operational regimes. The M3D-K code is a non-linear, δf code that can model the saturation amplitude of modes, frequency chirping and some forms of multimode coupling. Its future development will be within the recently approved energetic particle center lead by PPPL in collaboration with IFS and Colorado University. The much improved M3D-k code with the gyro-kinetic physics will be called GKM and will be able to model realistically the kinetic physics and the fast ion transport due to Alfvenic modes. The inclusion of gyro-kinetic physics is necessary for proper modeling of the coupling of Alfvén modes to kinetic Alfvén waves (KAW) where the eigenmodes enter the continuum, an important damping mechanism for TAE. The high-k scattering diagnostic on NSTX can directly measure the KAW waves, offering the exciting opportunity to study this physics.

An important part of the five year plan will be to utilize this capability to model well documented examples of Alfvénic instability induced fast ion losses. To supplement this effort, the NOVA-K and ORBIT codes will be used to simulate fast ion transport due to experimentally measured modes. NOVA-k calculates the linear mode eigenfunction, as well as drive and damping terms. The eigenfunctions calculated with NOVA can be normalized with experimental data and used in the particle tracking code, ORBIT, to calculate the affect on fast ion transport. These numerical simulations will then be compared to enhancements of fast ion transport as measured with FLIP, NPA and FIDA diagnostics.

A critical parameter of energetic particle-driven Alfven modes is the normalized gyroradius of energetic particles. It is known that beam-driven Alfven instability is maximized at $k_\theta * \rho_{hot} \sim 1$. The stability threshold is also expected to be affected due to the change in the damping from the thermal plasma. More importantly, the number of unstable mode is expected to increase strongly with decreasing energetic particle gyroradius. This can in turn affect energetic particle transport due to the increased number of unstable modes. The doubling of magnetic field in the NSTX upgrade would allow a parameter scan in the beam gyro-radius over a factor of 3. With the upgrade to the center-stack, we can investigate experimentally the ρ_{beam} dependence of the stability threshold, unstable mode spectrum, and beam ion transport for beam-driven TAE/EPM modes predicted theoretically. The results of this experiment will help us to understand energetic particle transport in the presence of multiple modes and will provide critical data for validating nonlinear energetic particle simulation codes for predicting alpha particle transport in ITER.

On NSTX the electron thermal speed is only a little higher than the fast ion speed, e.g., at 1 keV the electron thermal speed is only 4.5 times the speed of a 90 kV deuterium beam ion. Thus, it is not surprising that some significant populations of thermal electrons have resonant interactions with fast-ion driven instabilities such as CAE or GAE. Such an interaction, leading to increased diffusivity for the electrons, is being considered as an explanation for anomalously large electron heat diffusivity seen in some regimes on NSTX, an explanation supported by simulations with the ORBIT code. The higher electron temperatures, which might be expected to accompany higher field operation, would separate the velocity scales and clarify the physics of this phenomenon.

4.4.3 CAE Heating

Stochastic heating of magnetized ions or electrons with large amplitude waves at frequencies just below the cyclotron frequency was proposed in the mid '70's to the early '80's for a variety of modes [4.4.2-4.4.6]. This work was, perhaps, an outgrowth of earlier experiments and theoretical work on heating of plasmas with stochastic waves [4.4.19-4.4.23]. An extensive experimental study of stochastic ion heating by a large amplitude wave was done on the ENCORE tokamak by Paul Bellan's group between 1986 and 1998 [4.4.7-4.4.11]. Stochastic heating of thermal ions was measured with a laser-induced fluorescence diagnostic. The wave was a large amplitude drift-Alfvén wave [4.4.24], probably driven by the plasma current. In a fairly extensive set of experiments, good agreement was found with the theory of stochastic heating. Recently, numerical studies of stochastic ion heating were done in the context of CAE [4.4.25-4.4.26]

The broad spectrum of CAE and Global Alfvén Eigenmodes (GAE) modes in the proper frequency range on NSTX offers an opportunity for stochastic thermal ion heating. These natural modes are weakly damped, as evidenced by the ease with which they are excited by the neutral beam fast ion population. Based on measurements of the mode damping rate and wave amplitude, and assumptions about the wave localization, only a few 10's of kWs of power would be required to excite waves to the amplitudes that are seen. Numerical simulations have estimated that wave amplitudes 5 to 10 times higher than the peak so far observed would be necessary for stochastic ion heating. This power heats the electrons, as the damping is primarily electron Landau or continuum damping. A low linear damping rate means that relatively little power would be lost to the electrons by exciting the wave to the stochastic threshold amplitude, after which most of the additional heating power would be deposited in the thermal ion population. This thermal ion heating mechanism represents a form of alpha channeling [4.4.1] in that the GAE and CAE also take energy from the fast ion population and "channel" it to the thermal ion population, but with the additional possibility of some control via an externally excited antenna.

Experiments with a 5-10 kW, 0.1 - 1.5 MHz source to measure coupling to eigenmodes of the plasma would follow earlier experimental studies using antennas to launch Alfvén waves [4.4.27-4.4.29]. With 5 – 10 kW, it might also be possible to excite waves to the detection threshold of the microwave reflectometer systems on NSTX. The goal of these higher heating power experiments would be to further

understanding of the stochastic heating mechanism, rather than to see substantial ion heating. Further, excitation of Alfvén eigenmodes with a coil inside the vacuum vessel and a low power amplifier (≈ 5 kW) is a valuable tool for the study of mode stability [4.4.30]. The spectrum of stable modes can be detected and the linear damping rate measured directly. This is very helpful information as stability codes must calculate both the sum of the damping and drive terms, the difference of which is the linear drive for the mode. Thus a direct measurement of the linear damping term also helps to interpret the experimentally determined linear growth rate.

The experiments would be supplemented with numerical calculations, as is done for other forms of RF heating. An effort has begun to develop the full-wave TORIC code [4.4.31] for simulations of wave excitation with the HHFW antenna at frequencies below or near the ion-cyclotron frequency. The TORIC full wave code can complement traditional stability codes, such as HYMN, GKM (gyrokinetic version of M3D) or NOVA-K. TORIC includes finite Larmor radius effects, finite ω/ω_{ci}, cyclotron resonances and a fast ion population. Further, TORIC can attain higher spatial resolution, although in a linear model. Initial simulations have found three waves near the cyclotron frequency, one of which may be a core-localized GAE.

4.4.4 Status of Energetic Particle Research

Fishbones and EPMs:

Bursting, chirping modes are seen in NSTX with frequencies starting at over 100 kHz and which can chirp down 10's of kHz on a millisecond timescale [4.4.32-4.4.40]. These modes can be present with $q_{min} \geq 1$ and with, sometimes multiple, toroidal mode numbers $1 \leq n \leq 4$. In plasmas where $q_{min} \approx 1$, the modes typically have characteristics resembling the fishbone mode seen on conventional aspect ratio tokamaks. The modes are core-localized with a kink-like structure (no or small islands). Under conditions where q_{min} is believed to be well above unity, the modes often have toroidal mode numbers greater than one. The modes still appear to be core localized and kink-like in nature. Some of these modes have been identified as bounce-precession resonance fishbone modes. They are expected to be unstable in high current, low shear discharges where the conventional precession-resonance drive is weak (due to low precession drift frequency) [4.4.33]. These plasmas have a significant population of trapped

particles with a large mean bounce angle, produced by near tangential beam injection into a small aspect ratio device.

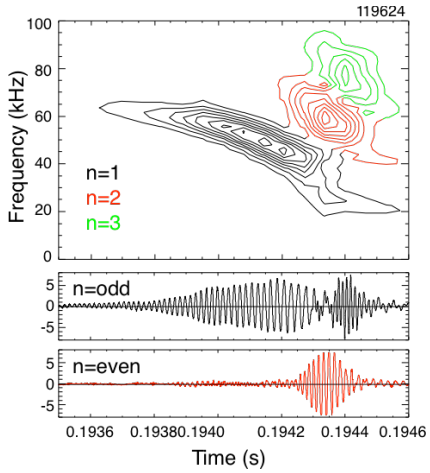

Figure 4.4.1: Fishbone mode showing multimode transport [4.3.38]

The strength of neutron drops (fast ion losses or transport) varies widely for these bursting, chirping modes. Those resembling the classical fishbone modes ($n = 1$, $q_{min} \approx 1$) are most reliably correlated with neutron rate drops. However, many of the bursts involve multiple modes, and in some cases transient losses of fast ions (directly measured with the scintillator Fast Lost Ion Probe, sFLIP) are correlated with periods when multiple modes are present [4.4.40] (see Fig. 4.4.1).

Additional experimental studies of the mode structure, stability boundaries and resonant drive are necessary to develop the ability to predict their appearance and affect on fast ion confinement. At present, even though the mode eigenfunction is relatively well known, simulation of the fast ion losses has not been done.

Toroidal Alfvén Eigenmodes and Avalanches:

Multiple TAEs are commonly observed in beam heated NSTX discharges. However, evidence for significant fast ion transport or loss appears confined to instances of strong, multimode bursts (*e.g.,* Fig. 4.4.2). Fast ion orbits are modified as they interact with the TAE, with those fast ions resonant with the wave becoming trapped in the wavefield, *i.e.,* forming "phase-space islands". As the mode amplitude increases, more fast ions will be trapped and the islands will become larger. It has been proposed that when the resonances from multiple modes are nearby in phase space, sufficiently large amplitude modes will cause the phase space islands to overlap. The orbits of the formerly trapped ions become

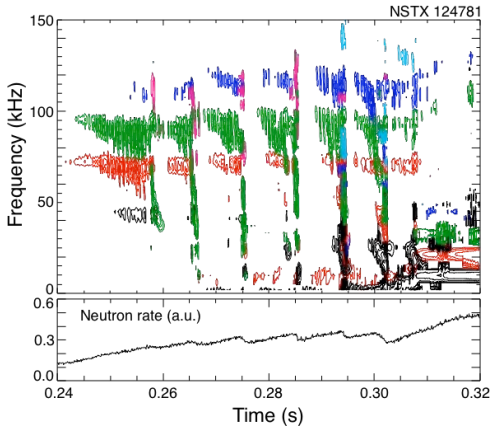

Figure 4.4.2: TAE avalanches and neutron drops indicating fast ion losses

stochastic and very rapid transport of fast ions may occur. Additionally, the ensuing modifications to the fast ion distribution function may result in otherwise stable modes being excited, ultimately leading to an "avalanche" effect which further enhances the transport of fast ions [4.4.13-4.4.17]. This mechanism of fast ion transport through an interaction of many modes could be important in ITER [4.4.12].

TAE avalanches, correlated with drops in the neutron rate suggesting fast ion losses, have been studied in NSTX. Recent experiments have documented the internal mode amplitudes, measured with the five-channel reflectometer system, together with MSE documentation of the current profile. These measurements provide the basis for numerical modeling of the island overlap threshold and enhanced fast ion transport. These experiments were necessarily carried out in L-mode plasmas to obtain reflectometer measurements of the internal structure. As with many of the studies of fast ion driven instabilities, it is important to extend these studies to the high performance, H-mode regimes, even at the expense of detailed measurements of the internal structure. The addition of the BES diagnostic will remove the requirement of L-mode density profiles for internal mode measurements, allowing Avalanche studies to be extended to the H-mode regime. The higher field available with the center-stack upgrade in 2012 will allow access to regimes with smaller $V_{fast}/V_{Alfvén}$ and ρ^*, extending the experimental basis for scaling of the Avalanche physics.

Simulations of the fast ion redistribution due to interactions of multiple toroidal Alfvén eigenmodes have been done with the M3D-k code [4.4.41]. These simulations demonstrated both the synergistic interaction of multiple modes, giving a higher saturation amplitude, and the "overlap" of islands from individual modes in fast-ion phase-space responsible for the larger saturation amplitude. In parallel, simulations are being done with the NOVA and ORBIT codes, using the experimentally observed mode spectrum and amplitudes to compare with measurements of fast ion losses.

Beta-induced Alfvén Acoustic Eigenmodes:

New global MHD eigenmode solutions have been found numerically below the Geodesic Acoustic Mode (GAM) frequency in gaps in the low frequency Alfvén-acoustic continuum [4.4.42, 4.4.43]. These new eigenmodes can explain observations of modes with frequencies well below the TAE frequency (Fig. 4.4.3). These global eigenmodes, referred to here as Beta-induced Alfvén-Acoustic Eigenmodes (BAAE), exist in the low magnetic safety factor region near the extrema of the Alfvén-acoustic continuum. In

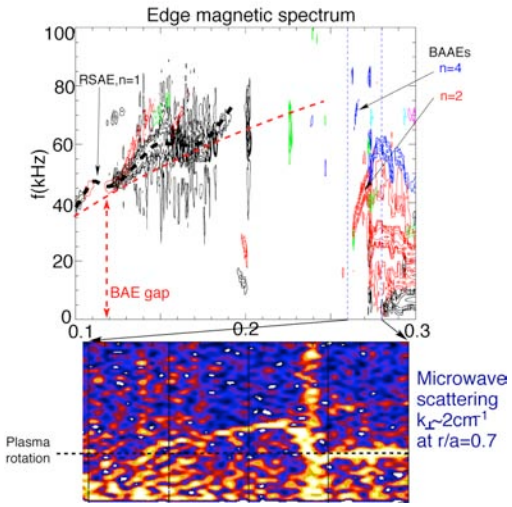

Figure 4.4.3: Beta-induced Alfvén Eigenmodes

accordance with the linear dispersion relation, the BAAE frequency increases as the safety factor, q, decreases. We show that BAAEs can be responsible for the observations of low frequency modes in relatively high $\beta > 20\%$ NSTX plasmas. In contrast to the mostly electrostatic character of GAMs, the new global modes also contain an electromagnetic (magnetic field line bending) component due to the Alfvén coupling, leading to wave phase velocities along the field line that are large compared to the sonic speed. Initial measurements with the high-k scattering diagnostics have found evidence of mode conversion to short wavelength kinetic Alfvén waves as the BAAE enters the continuum. The ability to make these measurements will be valuable in the study of other Alfvén waves as well. Qualitative agreement between theoretical predictions and observations are found.

Beta Dependence of Alfvén Cascade Modes:

Alfvén Cascade Modes have been found in low density, low β NSTX plasmas (Fig. 4.4.4). An extension of the theory of Cascade modes, that includes the coupling to the GAM [4.4.44-4.4.46], is shown to imply their absence for typical ST β's. A scan in β confirmed a threshold for suppression of Cascade modes in accord with theoretical predictions. Further, good agreement was found between the observed onset frequency and the frequency estimated from a simple dispersion relation for the GAM.

The time evolution of q_{min} as calculated from the observed mode frequency sweeping was also found to be in good agreement with that found from equilibrium reconstructions using measurement of the equilibrium magnetic field pitch. This measurement was made with the MSE diagnostic.

Some limited measurements have been made of the internal structure of these modes. Future experiments will try to improve on these measurements, with a view, in particular, of detecting changes in the mode structure as the Alfvén Cascade modes saturate at the TAE gap. Because these modes occur in low β, thus low density plasmas, new diagnostics such as the BES are required for detailed measurements of the internal structure and amplitude.

These studies have been primarily done in L-mode plasmas. It remains to be seen whether a sufficiently low β H-mode plasma can be made such that Alfvén Cascade modes would be present. Finally, no strong evidence has been found to connect these modes to enhanced fast ion transport as has been reported elsewhere. Future experiments could take a closer look at this issue.

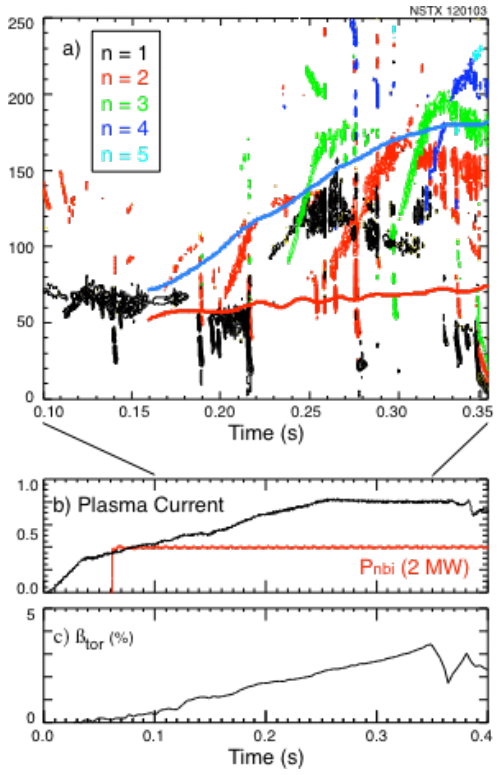

Figure 4.4.4: Alfvén Cascades

Compressional and Global Alfvén Eigenmodes and Angelfish (Hole-Clumps):

Neutral-beam-driven CAE at frequencies in the range $0.2\,\omega_{ci} \le \omega \le \omega_{ci}$ are commonly seen in NSTX plasmas [4.4.47-4.4.49]. The modes typically have a spectrum with multiple frequency peaks, sometimes equally spaced and with sequential toroidal mode numbers. The modes are counter-propagating for moderate mode numbers, $3 \le n \le 6$, and co-propagating for high mode numbers $9 \le n \le 13$. The frequency has a scaling with toroidal field and plasma density consistent with Alfvén waves. The modes have been observed with high bandwidth magnetic pick-up coils and with a reflectometer. The high-k scattering system has again, in some instances, detected coherent modes with frequencies matching those seen on the Mirnov coils, suggesting continuum damping through mode-conversion to kinetic Alfvén waves.

Alfvénic Bursts (AB) of either compressional or global Alfvén eigenmodes, with strong frequency chirps have been observed in the early neutral beam-heating phase of discharges (Fig. 4.4.5). The bursts last for < 0.3 – 0.7 ms, and the mode frequency chirps simultaneously up and down. The frequency evolution of the bursts is well described by the "Hole-clump pair" theory of Berk, Breizman, and Petviashvili, [4.4.50]. The AB arises from the generation of a hole in the particle distribution function, paired with a clump, and the non-linear interaction of the instability with the distribution function results in the propagation of the holes and clumps in phase space, which together with background damping, results in the simultaneous upward and downward frequency chirps of the mode. The hole-clump theory relates the rate of the frequency chirp to the linear damping rate of the mode. The damping rate determined by the frequency chirping is found to be in good agreement with predictions of the NOVA-k code.

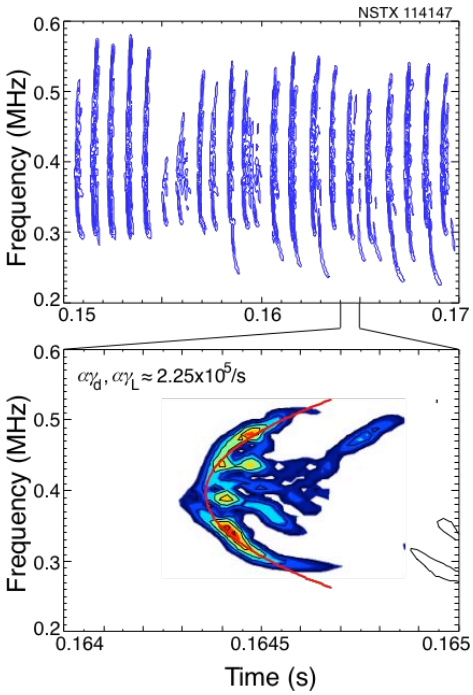

Figure 4.4.5: CAE hole-clumps (Angelfish)

There still remains ambiguity regarding the identification of these modes as GAE or CAE. Further numerical simulations and improvements in the measurement of the mode polarization, as well as internal structure with the multi-channel reflectometer system might help resolve this question. Likewise, additional work needs to be done to understand the extension of the hole-clump theoretical model to Doppler-shifted cyclotron resonance driven modes as these are believed to be.

Initial observations of sub-cyclotron frequency modes, $0.2\ \omega_{ci} \leq \omega \leq \omega_{ci}$, were interpreted as CAE. Simulations with the HYM code, however, found that both CAE and GAE should be expected for the parameters of typical NSTX plasmas. Evidence for this second type of mode was soon found. The peaks in the frequency spectrum for these new instabilities intersect each other as plasma parameters evolve, whereas the CAE spectral peaks, which depend only upon density, tend to evolve parallel to each other.

The shear Alfvén dispersion, $\omega \approx k_{||} V_A$, $k_{||} = (m - nq)/qR$ allows for more complex behavior as the q profile and density are evolving independently during the discharge. A theory of localized CAEs and GAEs in low aspect ratio plasmas explains the observed high frequency instabilities [4.4.26,4.4.51-4.4.61]. Both classes of modes may be excited through the velocity space gradient of energetic super-Alfvénic beam ions via Doppler shifted cyclotron resonances (or, in the case of CAE, directly through a parallel bump-on-tail). CAE modes were also found on DIII-D in an aspect ratio scaling experiment motivated by the NSTX observations [4.4.62].

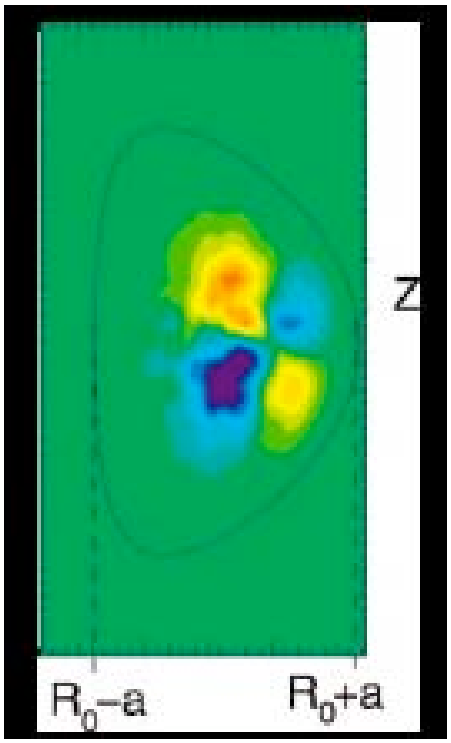

Figure 4.4.6: Color Contours of the fluid pressure perturbation of n = 4, m = 2 GAE mode plotted in the poloidal R , Z plane. Shown also is the last closed magnetic surface of the NSTX plasma. The red color regions indicate the high perturbed pressure, whereas dark blue ones correspond to the negative value of the pressure perturbation.

Non-linear, three-dimensional 3D hybrid simulations using the HYM code have been employed to study the excitation of both CAE and GAE by energetic ions in NSTX. The HYM simulations for typical NSTX parameters find that GAE are the most unstable modes, for low toroidal mode numbers, $2 \le n \le 7$ at the large injection velocities of beam ions, $V_b \approx 3V_A$. The GAE are localized near the magnetic axis, and have large $k_{||}$, so that $\omega \approx k_{||} V_{b||} \approx \omega_{ci}/2$. The perturbed plasma pressure in the poloidal cross-section of an NSTX plasma due to a GAE with $n = 4$ and $m = 2$ is shown in Fig. 4.4.6. These modes also have a significant compressional component, $B_{||} \approx B_{\perp}/3$, due to strong coupling to the compressional Alfvén wave. In the HYM simulations for $n_b/n_p \approx 3\%$, the growth rates of the unstable GAEs are found to be of the order $\gamma/\omega_{ci} \approx 0.002 - 0.01$ with frequencies $\omega/\omega_{ci} \approx 0.3 - 0.5$, where ω_{ci} is evaluated at the magnetic axis.

Stochastic Ion Heating:

With strong neutral beam heating in NSTX a broad spectrum of fluctuations is observed in the frequency range from about 0.2 to 1.2 times the ion cyclotron frequency, demonstrating that there are many weakly damped eigenmodes present for stochastic ion heating. The modes have been identified as CAEs or GAEs. The linear damping rate has been determined from non-linear behavior of the mode frequency under some conditions, and calculated with NOVA-K and HYM.

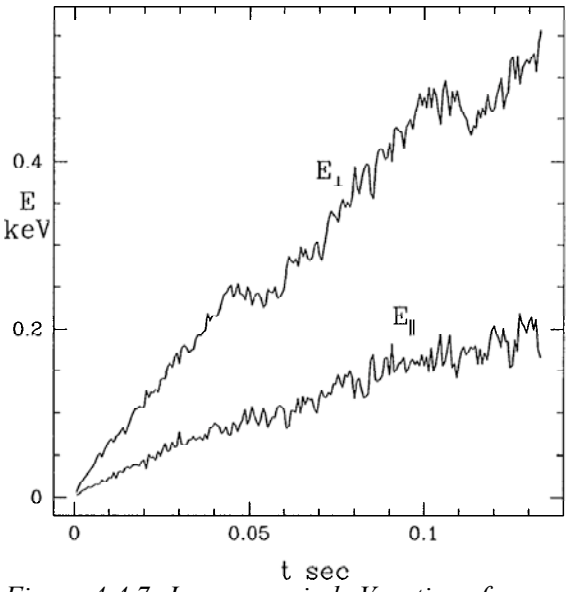

Figure 4.4.7: Ion energy in keV vs time, for $dB_y/B = 6.0x10^{24}$.

We simulated this effect in a more complex toroidal geometry [see figure 4.4.7] than was reported previously [4.4.25, 4.4.26]. Stochastic domains at low energy corresponding to the plasma background ions occurs at a lower amplitude than in the slab plasma. The initial temperature profile of thermal ions is shown as a solid parabolic curve in figure 4.4.7. We used 21 CAEs to simulate the measured CAE spectrum by edge Mirnov probes in NSTX. Internal measurements of the rms amplitude of the perturbations is not available and was fixed at $\delta B / B = 0.5 \times 10^{-3}$ in calculations with the collisional frequency $\nu = 0.01\omega_c$. Mode frequencies were in the range $0.2 < \omega/\omega_{ci} < 0.8$. Calculations indicate that the heating is proportional to the mode numbers if the amplitude is fixed. Stochastic multimode heating by CAEs could provide a way of direct energy channeling from beam ions (fusion alphas) to the thermal plasma ions.

Non-linear Multi-mode Coupling:

Simultaneous bursts of Energetic Particle Mode (EPM) and TAE activity that correlate with significant fast-ion loss are observed in beam-heated plasmas. Three-wave interactions between these modes have been conclusively identified, indicating fixed phase relationships [4.4.18]. This nonlinear coupling concentrates the energy of the TAEs into a toroidally localized perturbation frozen in the frame of a rigid,

toroidally rotating structure formed by the EPMs. This redistribution of energy is significant because it will modify the effect of the TAEs on fast-ion loss.

Measurements of MHD-induced Energetic Ion Transport or Loss:

In quiescent or MHD-benign NSTX discharges, NPA measurements of the energetic beam ion distribution are consistent with classical behavior [4.4.63]. The appearance of strong, bursting or continuous MHD or Alfvénic activity can significantly affect the energetic (E ~ 10 – 100 keV) deuterium ion population. Evidence of MHD-induced energetic ion transport or loss in NSTX relies primarily on neutron rate and charge exchange Neutral Particle Analyzer (NPA) [4.4.64] measurements. Neither the volume integrated neutron rate nor the line-integrated NPA effux, however, can distinguish between transport or loss so additional diagnostics, such as sFLIP, FIReTIP and USXR are used to augment these measurements. sFLIP is able to identify ion loss while the others serve to spatially localize MHD-activity for the purpose of analysis using the time, space and energy dependent Anomalous Fast Ion Diffusion (AFID) model in TRANSP that is used to emulate MHD-driven transport or loss of energetic ions. Comparison of MSE-reconstructed toroidal current profiles with calculations taking into account AFID redistribution of NBI driven current helps to identify fast ion redistribution [4.4.65]. The AFID model is iterated to simultaneously match measurements of the neutron yield, NPA change exchange efflux and MSE reconstructed current profiles with the TRANSP simulation.

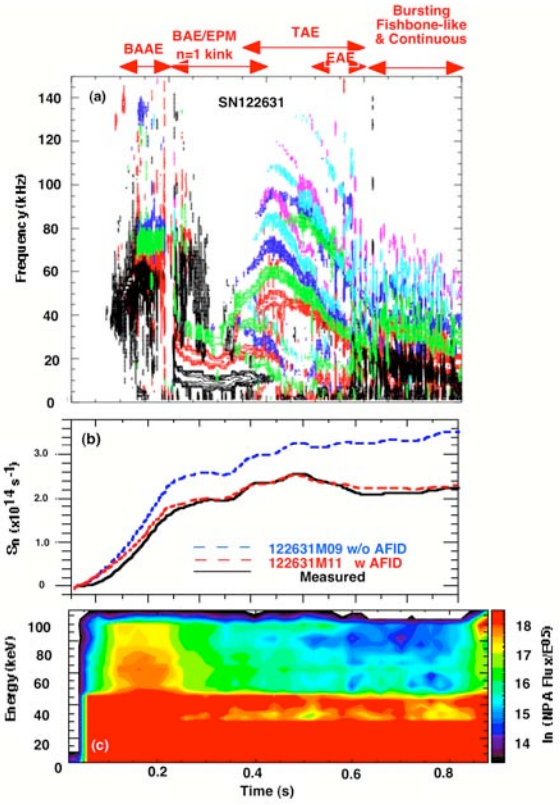

Figure 4.4.8: Mirnov MHD spectrogram, (a) measured and TRANSP-calculated neutron rates (b) and NPA energetic ion spectrum(c) for a typical H-mode discharge in NSTX.

Although redistribution or loss of energetic ions due to low-frequency (f ~ 10 kHz) kink-type MHD activity has been reported previously [4.4.66], the primary goal of recent work [4.4.67] has been to contrast redistribution or loss due to continuous Energetic Particle Modes (EPM) and Toroidal Alfvén Eigenmode (TAE) activity (f ~ 20 – 150 kHz) modes with the low-f MHD modes, a topic that heretofore has not been investigated in detail for NSTX plasmas.

A NPA vertical scan was performed for a series of reproducible H-mode discharges, some characteristics of which are shown in Fig. 4.4.8. In panel (a), the Mirnov spectrogram shows robust activity in the low frequency range (f ~ 0 – 150 kHz) where continuous f < 20 kHz kink-type activity and bursting fishbone-like activity are intermingled with a 'sea of Alfvénic modes'. A tentative classification of the mode activity is presented in the header. Panel (b) illustrates the typical disparity in neutron yield for H-modes having strong MHD activity wherein the normal TRANSP-calculated rate (blue curve exceeds measurement (black curve), often by as much as 50±20%. The TRANSP-calculated rate using the AFID model (red curve) provides agreement with the measurement. Panel (c) shows a contour plot of the NPA efflux where it can be seen that energetic ion depletion above E > $E_b/2$ starts around t ~ 150 ms (coincident with onset of strong MHD activity) and grows throughout the discharge.

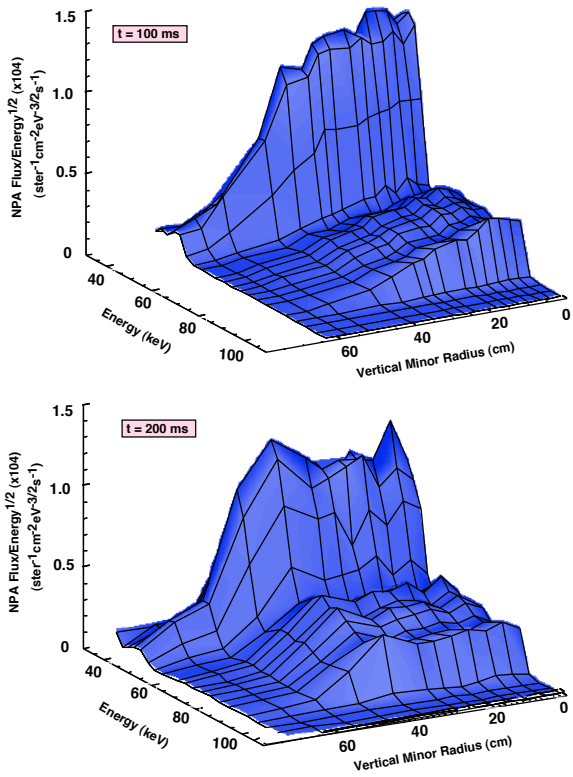

Figure 4.4.9: NPA vertical scan energetic ion spectra during MHD-quiescent (top panel) and MHD-active (bottom panel) discharge periods.

Selected NPA vertically scanning results are shown in Fig. 4.4.9 where the vertical minor radius axis is the distance along a vertical line centered at the intersection of the NPA sightline with the NB footprint (where the NPA efflux is

localized by charge exchange on the beam primary and halo neutrals). The NPA flux is displayed on a linear z-axis and the larger efflux at lower energy is the E/2 component of the neutral beam. The spectrum in the top panel corresponding to a MHD-quiescent period (dB ~ 10^{-2} Gauss) at t ~ 100 ms shows a monotonically decreasing energetic ion distribution from the core outwards. By contrast, during strong MHD activity (dB ~ 10^{-1} Gauss) at t ~ 200 ms the energetic ion distribution in the core region is depleted and the core ions are redistributed radially outwards to form a 'shoulder' on the measured distribution as evident in the bottom panel. Following this initial redistribution, the NPA spectra continue to exhibit depletion throughout the duration of the ~ 800 ms discharge. This depletion is due in part to attenuation of the charge exchange neutral efflux with increasing plasma density and in part to MHD-induced energetic ion redistribution. TRANSP analysis is used to separate these contributions.

The sFLIP and FIReTIP signal activities (not shown) correlate with the Mirnov coil continuous low frequency (f < 20 kHz) MHD activity (along with sporadic bursting fishbone-like activity). sFLIP energetic ion loss and FIReTIP $\delta n_e/n_e$ core fluctuations are conspicuously absent during higher-frequency continuous TAE and CAE/GAE activity in the time interval t ~ 0.43 – 0.9 s except possibly for MHD bursting activity at t ~ 0.78 s and t ~ 0.83 s. The leads to a tentative conclusion that both bursting fishbone-like and low-f kink-type MHD modes drive energetic ion loss whereas continuous TAE-like Alfvénic modes at most cause redistribution and the energetic ions remain confined [4.4.67].

So far, the role regarding energetic ion redistribution or loss of higher-frequency (f ~ 200 – 2000 kHz) CAE/GAE activity that is omnipresent during NSTX H-mode discharges cannot be separated from the lower-frequency activity (f ~ 0 – 100 kHz). Certainly they perturb the part of the fast ion distribution responsible for exciting them. While the typical amplitudes of the magnetic fluctuations are 1 – 2 orders of magnitude below those for the lower frequency fluctuations, the frequency may be an order of magnitude higer, so their role in fast ion redistribution remains to be verified.

4.4.5 Energetic Particle Research Plan for 2009-2013

The additional diagnostic capabilities and expanded parameter range (toroidal field up to 1 T) will greatly improve our understanding of the nature and impact of fast ion driven instabilities and our ability to validate numerical codes used to predict fast ion behavior in future devices.

New diagnostics include improvements to fast ion diagnostics such as the addition of the FIDA diagnostic to measure confined fast ion distributions and higher speed sFLIP data, either through a fast camera, or as a finite number of fast photomultiplier channels to improve correlation of losses with fast ion instabilities. In the post-2010 time frame, a neutron collimator could provide additional important measurements of fast ion redistribution. Improvements are planned for the reflectometer system, which is presently the basic diagnostic for internal measurements of mode structures and amplitudes. An upgrade to higher bandwidth is planned for the tangential interferometers, which could provide information on mode amplitudes in H-modes, something not possible with the reflectometers. A BES diagnostic , which could complement the reflectometer measurements will be added in 2009. The high-k scattering diagnostic has not been fully exploited for studies of kinetic Alfvén waves (KAWs), a result of continuum damping of Alfvén modes. In the following schedule we list some experimental goals that might optimistically be achieved in the experimental campaigns of 2009 and 2010

2009:

In the 2009 campaign we propose experiments to continue studies of the wide range of energetic particle driven instabilities, with emphasis on their effect on beam driven current distributions. The FIDA diagnostic should be fully operational, and there may be some data available from the BES diagnostic. The MSE-LIF diagnostic may simplify experiments requiring measurement of the q-profile evolution as the restrictive requirement for beam source A at 90 kV to get MSE data will be lifted. The use of non-resonant magnetic field braking is a capability of NSTX that hasn't been fully exploited and could contribute to these experiments.

The highest priority will be to complete validation of numerical models for predicting fast ion transport as measured in studies of the TAE avalanches for present NSTX parameters (3.5 kG to 5.5 kG). Experiments will address the scaling of the onset thresholds with q-profile, fast ion distribution (pitch angle, energy) and $V_{fast}/V_{Alfvén}$ through density and toroidal field scans. The neutral beam voltage and source dependence of TAE avalanches, a high priority in terms of impact on fast ion transport, would be investigated. An experiment will be dedicated to producing TAE modes and a search for continuum damping via coupling to KAW will be made using the high-k scattering diagnostic. Careful documentation of the current profile evolution will be done.

The study and modeling of the impact of EPMs on beam driven currents will begin in earnest with the improved diagnostic capability. The parametric dependencies of these modes on q-profile and beta will be investigated. The FIDA and BES diagnostics will be used to document the internal mode structure and redistribution of fast ions. The role of drift-reversal, assumed to be an important stabilizing effect for ITER, will be studied. Mode structure measurements will be used to validate the NOVA and PEST linear ideal codes as well as the M3D-K non-linear code. Predictions of fast ion transport with ORBIT and M3D-K will be compared with experimental data.

Documentation of the Alfvén Cascade eigenmode evolution to TAE modes will be completed. Density, toroidal field, and beam voltage scans will help to identify the parametric scaling of the GAM frequency from which the effective specific heat for the fast ion distribution can be determined. The data will provide important validation of the NOVA and M3D codes for plasmas with reversed core magnetic shear.

Complete documentation of internal mode structure and begin scaling of threshold parameters of the beta-induced Alfvén Acoustic mode (BAAE) will continue, utilizing the high-k scattering and BES diagnostics.

Finally, the first experiments to measure CAE/GAE coupling to an existing HHFW antenna strap will be done. This will provide useful information on the design of a dedicated CAE antenna.

2010:

The fast Mirnov arrays will be upgraded for the 2010 campaign for increased bandwidth compatible with higher mode frequencies expected with the center stack upgrade and to provide additional spatial coverage. Additionally, the FIDA diagnostic to measure distributions of confined fast ions and the BES diagnostic for measurement of internal mode structure should be routinely available.

In this year the fast ion transport code validation emphasis will be extended to the study of Alfvén Cascade modes and to TAE avalanches in H-mode plasmas, utilizing the BES diagnostic for internal measurements of mode structure and amplitude. This is an important regime in which to understand the modes, and the flatter density profile could play an important role in the physics of the modes. The

addition of the BES diagnostic gives us the important ability to measure the internal mode amplitude and structure needed to validate numerical models.

The impact of fishbones on beam driven currents will be revisited with the improved diagnostic capability. The parametric dependencies of these modes on q-profile and beta will be investigated. The BES and FIDA (and other fast ion diagnostics) diagnostics will be used to document the internal mode structure and redistribution of fast ions. The role of drift-reversal, assumed to be an important stabilizing effect for ITER, will be studied.

There will be an experiment dedicated to the study of three-wave coupling between fishbone-like modes, TAE and the higher frequency GAE/CAE. Three wave coupling between these modes could affect instability thresholds as well as particle transport. Again, the BES system would contribute to this experiment. The FIDA diagnostic, together with sFLIP and NPA, will be used to look for fast ion redistribution correlated with three-wave coupling.

Additionally, the sensitivity of TAE avalanches to He-D concentration ratios will be studied. This may provide some insight into damping mechanisms for TAE modes. The switch from D to He both lowers the thermal ion speed as well as lowering the thermal ion beta (for fixed electron density), changing the ion Landau damping term for the TAE modes.

A number of the previous experiments, notably those on BAAEs and Alfvén Cascades, could benefit from the use of HHFW to control the electron temperature, thus altering the role of the Acoustic mode coupling for these modes.

The first low power coupling experiments to Alfvén waves will be done using an existing HHFW strap and a low power amplifier.

2011-2013:

The upgrade to the center stack will allow operation to toroidal fields of up to 1 T, and plasma current up to 2 MA. The higher field extends the range of $V_{fast}/V_{Alfvén}$ and ρ^* for scaling studies of the *AE activity, especially for the scaling of TAE avalanches closer to ITER parameters. The higher field may allow use of the full voltage and power capability of the neutral beams, extending the energy of the fast ions up to ≈ 110 kV. The ability to explore lower $V_{fast}/V_{Alfvén}$ is important as both present theoretical understanding

and experimental results suggest that the drive for TAE, and thus TAE avalanches, peaks for $V_{fast}/V_{Alfvén} \approx 2$. The increased range of ρ* will extend the studies of TAE avalanches by changing the range of poloidal harmonics and number of interacting modes, providing better validation of the NOVA/ORBIT and M3D-K (GKM) codes. The new center stack will allow experiments to explore fast ion parameters ranging from those expected for the CTF-ST down to parameters expected for ITER and NHTX. These experiments will be used to validate the scalings developed in lower field operation. The increase in parameter regime will provide an important test of the predictive capability of numerical models.

Compressional and Global Alfvén eigenmodes are predominantly excited through a Doppler-shifted ion cyclotron resonance, $\omega \approx \omega_{ci} - k_{||} V_{f||}$, a form of drive for these modes probably unique to STs. The extension of $V_{fast}/V_{Alfvén} => 1$ (relevant for ITER and NHTX) will open the possibility of the simpler resonant drive $\omega \approx k_{||} V_{f||}$, tapping more fast-particle free energy. The higher field and current from the center stack upgrade will probably have little impact on stability of energetic particle modes (e.g., fishbones), but the additional beam line will allow for some control of the fast ion spatial and pitch-angle distributions.

The neutron collimator will provide additional high quality information on redistribution of fast ions by energetic particle driven instabilities. The second neutral beam line will greatly extend the range of fast ion anisotropies The high frequency upgrade to Firetip should provide some internal mode amplitude and localization data for CAE/GAE frequency modes in H-mode plasmas. An experiment dedicated to the study of CAE/GAE hole-clumps, which provides important understanding of fast ion phase space transport, as well as tests present understanding of the non-linear behavior of energetic particle modes, will document the internal structure, as well as for the first time provide information on the poloidal localization of the modes and on the outboard local wavelength. Then an experiment will study the suppression of hole-clumps during HHFW heating to understand whether this reflects changes in the equilibrium plasma, or direct changes to the fast ion distribution. The BAAE modes will be revisited with the improved diagnostics to get better mode structure measurements and measurements of fast ion transport.

2009 – 2013 Timeline for HHFW/ECW/EBW Research

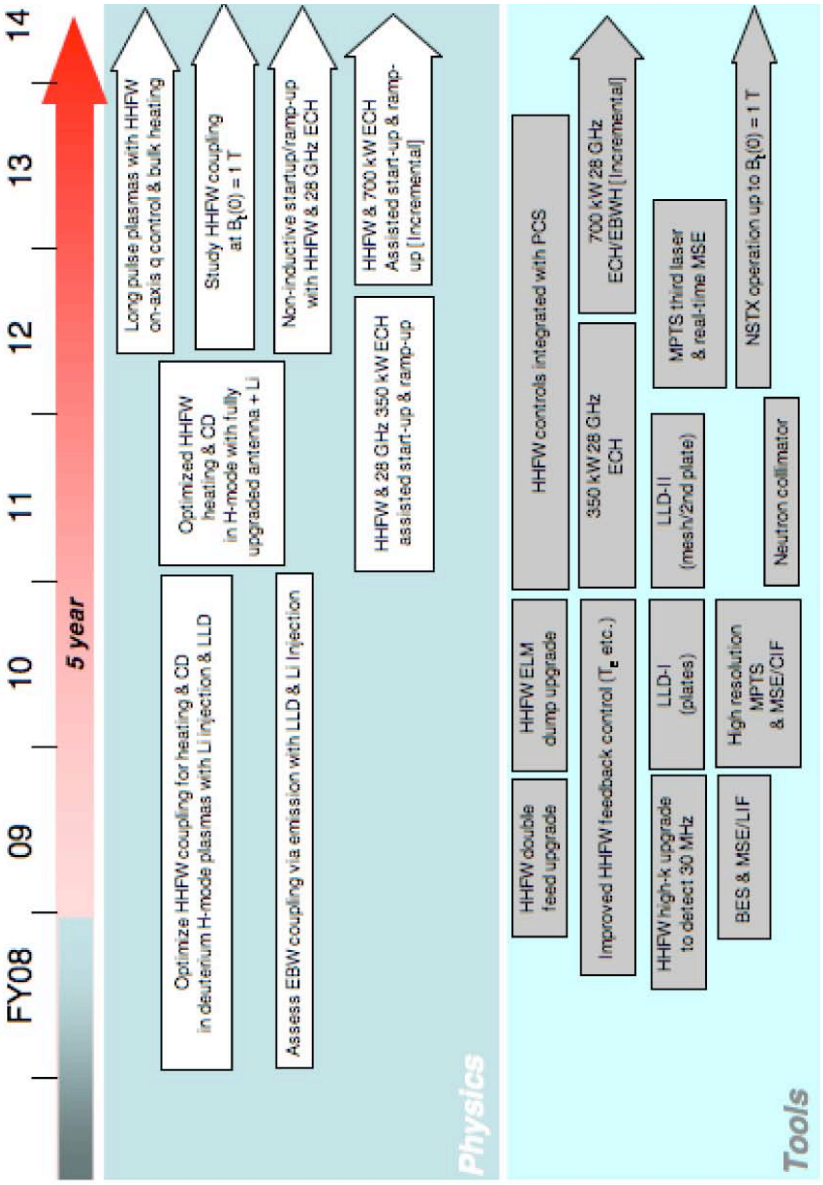

2009 – 2013 Timeline for Energetic Particle Research

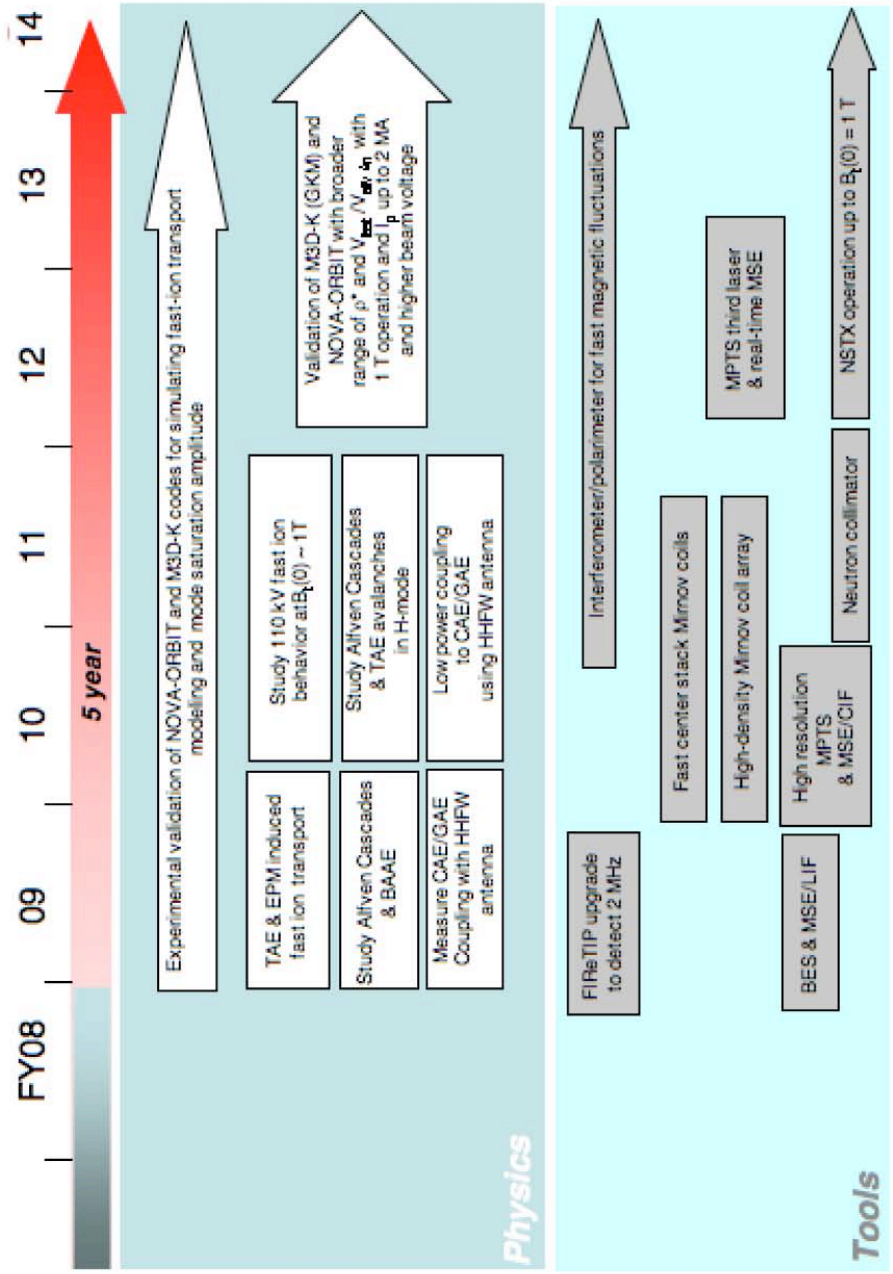

References

4.2.1 M. Ono, Physics of Plasmas **2**, 4075 (1995).

4.2.2 J. R. Wilson, *et al*., *16th Topical Conf. on RF Power in Plasmas*, AIP Conf. Proc. **787**, 66 (2005).

4.2.3 J. Hosea, *et al*., *17th Topical Conf. on RF Power in Plasma,* AIP Conf. Proc. **933**, 107 (2007).

4.2.4 J. Hosea, *et al*., Phys. Plasmas **15**, 056104 (2008).

4.2.5 A. P. Smirnov and R. W. Harvey, Bull. Amer. Phys. Soc. **40**, 1837 (1995); CompX Report CompX-2000-01 (2001).

4.2.6 E. F. Jaeger, *et al*., Nucl. Fusion **46**, S397 (2006).

4.2.7 A. L. Rosenberg, *et al*., Phys. Plasmas **11**, 2441 (2004).

4.2.8 J. Hosea, *et al*., *16th Topical Conf. on RF Power in Plasmas*, AIP Conf. Proc. **787**, 82 (2005).

4.2.9 J. B. Parker, *et al.,* Bull. Amer. Phys. Soc. **52**, 155 (2007)

4.2.10 P. T. Bonoli*, et al., 17th Topical Conf. on RF Power in Plasmas,* AIP Conf. Proc. **933**, 435 (2007).

4.2.11 P. M. Ryan, *et al*., Fusion Eng. and Design **56-57**, 569 (2001).

4.3.1 C. E. Kessel, *et al.*, Nucl. Fusion **45**, 814 (2005).

4.3.2 Y-K. M. Peng, *et al.*, Plasma Phys. Control. Fusion **47**, B263 (2005).

4.3.3 I. B. Bernstein, Phys. Rev. **109**, 10 (1958).

4.3.4 A. K. Ram, and S.D. Schultz, Phys. Plasmas **7**, 4084 (2000).

4.3.5 J. Preinhaelter and V. Kopécky, J. Plasma Phys. **10**, 1 (1973).

4.3.6 E. Mjølhus, J. Plasma Phys. **31**, 7 (1984).

4.3.7 F. R. Hansen, *et al*, J. Plasma Phys. **39**, 319 (1988).

4.3.8 C. B. Forest, *et al*., Phys. Plasmas **7** 1352 (2000).

4.3.9 N. J. Fisch and A. Boozer, Phys. Rev. Lett. **45**, 720 (1980).

4.3.10 T. Ohkawa, National Technical Information Service Report No. PB2000-108008, 1976 and General Atomics Report No. GA-A13847, 1976].

4.3.11 A. K. Ram, A. Bers, and C. N. Lashmore-Davies, Phys. Plasmas **9**, 409 (2002)

4.3.12 G. Taylor, *et al.*, Phys. Plasmas **12**, 052511 (2005).

4.3.13 J. Preinhaelter, *et al.*, AIP Conf. Proc. **787**, 349 (2005).

4.3.14 S. J. Diem, *et al*., Rev. Sci. Instrum. **77**, 10E919 (2006).

4.3.15 S. J. Diem, *et al*., *17th Topical Conf. on RF Power in Plasma,* AIP Conf. Proc. **933**, 331 (2007).

4.3.16 H. P. Laqua *et al.*, Phys. Rev. Lett. **78**, 3467 (1997).

4.3.17 V. Schevchencko , *et al*., Fusion Sci. Tech. **52**, 202 (2007).

4.3.18 V. Schevchencko , *et al*., AIP Conf. Proc. **933**, 323 (2007).

4.3.19 A. Mueck, *et al*., Fusion Sci. Tech. **52**, 221 (2007).

4.3.20 A.P. Smirnov, and R.W. Harvey, Bull. Am. Phys. Soc. **40**, 1837 (1995).

4.3.21 R.W. Harvey, and M.G. McCoy, *Proceedings of the IAEA Technical Committee on Advances in Simulation and Modeling of Thermonuclear Plasmas*, Montreal, Quebec (International Atomic Energy Agency, Vienna, 1993), p. 489; USDOC NTIS Doc. No. DE93002962.

4.3.22 G. Taylor, *et al.*, Phys. Plasmas **11**, 4733 (2004).

4.3.23 R.W. Harvey and G. Taylor, Phys. Plasmas **12**, 051509 (2005).

4.3.24 J. S. McKenzie, M.R. O'Brien and M. Cox, Comp.Phys.Comm. **66**, 194 (1991).

4.3.25 A. N. Saveliev, AIP Conf. Proc. **871**, 215 (2006).

4.3.26 A. K. Ram, J. Decker and Y. Peysson, *Proc. 14th Joint Workshop on ECE and ECRH*, (Santorini, Greece, May 2006) ed. Avrilios Lazaros (Heliotopos Conferences Ltd., Athens, Greece, 2006) p. 250.

4.4.1 N. J. Fisch and J.-M. Rax, Phys. Rev. Lett., **69**, 612 (1992)

4.4.2 G. R. Smith and A.N. Kaufman, Phys. Rev. Lett. **34**, 1613 (1975).

4.4.3 C. F. F. Karney and A. Bers, Phys. Rev. Lett. **39**, 550 (1977).

4.4.4 C. F. F. Karney, Phys. Fluids **21**, 1584 (1978).

4.4.5 J. Y. Hsu, K. Matsuda, M. S. Chu and T. H. Jensen, Phys. Rev. Lett. **43**, 203 (1979).

4.4.6 J. F. Drake and T. T. Lee, Phys. Fluids **24**, 1115 (1981).

4.4.7 J. M. McChesney, R. A. Stern, P. M. Bellan, Phys. Rev. Lett. **59** , 1436 (1987).

4.4.8 J. M. McChesney, P. M. Bellan and R. A. Stern, Phys. Fluids B **3** , 3363 (1991).

4.4.9 A. D. Bailey III, P. M. Bellan and R. A. Stern, Phys. Plasmas **2 ,** 2963 (1995).

4.4.10 A. D. Bailey III, R. A. Stern, and P. M. Bellan, Phys. Rev. Lett. **71**, 3123 (1993).

4.4.11 S. J. Sanders, P. M. Bellan, R A Stern, Phys. Plasmas **5** , 716 (1998).

4.4.12 N. N. Gorelenkov, H.L. Berk, and R.V. Budny, Nucl. Fusion **45**, 226 (2005).

4.4.13 E. D. Fredrickson, *et al.*, Nucl. Fusion **46**, s926 (2006).

4.4.14 H.L. Berk, B.N. Breizman and H. Ye, Phys. Lett. A **162**, 475 (1992).

4.4.15 H. L. Berk, B. N. Breizman, J. Fitzpatrick and H. V. Wong Nucl. Fusion **35**, 1661 (1995).

4.4.16 H. L. Berk, B. N. Breizman and M. Pekker, Nucl. Fusion **35**, 1713 (1995).

4.4.17 H. L. Berk, B. N. Breizman and M. Pekker, Phys. Rev. Lett. **76**, 1256 (1996).

4.4.18 N. A. Crocker, *et al*., Phys. Rev. Lett. **97**, 045002 (2006).

4.4.19 T. H. Stix, Phys. Fluids **7**, 1960 (1964).

4.4.20 S. Puri, Phys. Fluids **9**, 2043 (1966).

4.4.21 S. Puri, D. A. Dunn, and K. I. Thomassen, Phys. Fluids **11**, 2728 (1968).

4.4.22 S. Q. Mah, H. M. Skaragard, and A. R. Strilchuk, Phys. Rev. Lett. **25** 1409 (1970).

4.4.23 A. Hirose, S. Q. Mah, H. M. Skarsgard, A. R. Strilchuk, Phys. Fluids **17**, 2147 (1974).

4.4.24 E. D. Fredrickson and P. M. Bellan, Phys. Fluids **28**, 1866 (1985).

4.4.25 D. Gates, R. White, and N. Gorelenkov, Phys. Rev. Lett. **87**, 205003 (2001).

4.4.26 N. N. Gorelenkov, *et al*., Nucl. Fusion, **43**, 228 (2003).

4.4.27 G. Besson, *et al*., Plasma Phys. and Cont. Fusion **28**, 1291(1986).

4.4.28 G. A. Collins, *et al*., Phys. Fluids **29**, 2260 (1986).

4.4.29 A. B. Murphy, Plasma Physics and Cont. Fusion **31**, 21 (1989).

4.4.30 A Fasoli, *et al.*, Plasma Phys. Control. Fusion 44 (2002) B159–B172

4.4.31 M Brambilla, Plasma Phys. Control. Fusion **44** (2002) 2423.

4.4.32 E. D. Fredrickson, *et al*., *Proc. of 29th EPS Conf. on Controlled Fusion and Plasma Physics*, Montreaux, 2002, (the European Physical Society, Geneva) ECA vol. 26B (2002), P-1.104.

4.4.33 E D Fredrickson, L. Chen, and R. B. White, Nucl. Fusion **43**, 1258 (2003).

4.4.34 E. D. Fredrickson, *et al*., Phys. of Plasmas **10**, 2852 (2003).

4.4.35 S. Kaye, *et al*., Phys. Plasmas **10**, 3953 (2003).

4.4.36 Ya. I Kolesnichenko, VS Marchenko and R B White, Phys. of Plasmas **13**, 052504 (2006).

4.4.37 W. W. Heidbrink, *et al*., Plasma Phys. Control. Fusion **48**, 1347 (2006).

4.4.38 D. S. Darrow, *et al*., *Proc. 19th IAEA Fusion Energy Conference, Lyon, France, 14-19 Oct 2002* (IAEA, Vienna)

4.4.39 H. L. Berk, *et al*., Synopsis for 2006 IAEA meeting

4.4.40 D. Darrow, *et al*., *Proc. 34th European Physical Society Conference on Plasma Physics* (Warsaw, Poland June 2-6, 2007), paper p1.117.

4.4.41 G-Y Fu, et al, " *Nonlinear Hybrid Simulations of Multiple Energetic Particle driven Alfven Modes in Toroidal Plasmas*", 2007 APS DPP meeting, invited talk BI2/4.

4.4.42 N. N. Gorelenkov, *et al*., *Proc. for the 34th European Physical Society Conference on Plasma Physics* (Warsaw, Poland June 2-6, 2007) paper I3.006.

4.4.43 N. N. Gorelenkov, *et al*., submitted to Phys. Lett. A (2007).

4.4.44 B. N. Breizman and M. S. Pekker, Phys. Plasmas **12**, 112506 (2005).

4.4.45 E. D. Fredrickson, *et al*., *Proc. for the 34th European Physical Society Conference on Plasma Physics* (Warsaw, Poland June 2-6, 2007) paper p1.106.

4.4.46 E. D. Fredrickson, *et al*., "*Beta suppression of Alfvén Cascade Modes in the National Spherical Torus Experiment*" (accepted for Physics of Plasmas, 2007).

4.4.47 H. L. Berk, *et al*., "*Interpretation of Mode Frequency Sweeping in JET and NSTX", Synopsis for 2006 IAEA meeting*

4.4.48 E. D. Fredrickson, *et al*., Phys. of Plasmas **13**, 056109 (2006).

4.4.49 E. D. Fredrickson, *et al*., "*Observation of Hole-Clump Pair Generation at Compressional and Global Alfvén Eigenmode Frequencies"* (to be submitted to Physics of Plasmas, 2007)

4.4.50 H. L. Berk, B. N. Breizman and N. V. Petviashvili, Phys. Lett. A **234**, 213 (1997).

4.4.51 E. D. Fredrickson, *et al*., Phys. Rev. Lett. **87**, 145001 (2001).

4.4.52 N. N. Gorelenkov, C Z Cheng, and E Fredrickson, Phys. Plasmas **9**, 3483 (2002).

4.4.53 E. D. Fredrickson, *et al*., Phys. of Plasmas **9**, 2069 (2002).

4.4.54 N. N. Gorelenkov, *et al*., Nucl. Fusion **42**, 977 (2002).

4.4.55 N. N. Gorelenkov, *et al*., *Proc. 9th IAEA Fusion Energy Conference, Lyon, France, 14-19 Oct 2002* (IAEA, Vienna) paper IAEA-CN-94/TH/7-1 Ra

4.4.56 N. N. Gorelenkov, *et al*., Nucl. Fusion, **43**, 228 (2003).

4.4.57 E. Belova, *et al*., *"Numerical Study of Instabilities Driven by Energetic Neutral Beam Ions in NSTX*" in *Proc. of the 30th European Physical Society Conference on Controlled Fusion and Plasma Physics* (St. Petersburg, Russia, July 2003).

4.4.58 V. S. Belikov *et al*., Phys. of Plasmas **10**, 4771 (2003).

4.4.59 E. D. Fredrickson, N. N. Gorelekov and J. Menard, Phys. of Plasmas **11**, 3663 (2004).

4.4.60 E. Hameiri, A. Ishizawa and A. Ishida, Phys. Plasmas **12**, 072109 (2005).

4.4.61 Ya. Kolesnichenko, R. B. White, and Yu. V Yakovenko, Phys.of Plasmas **13**, 122503 (2006).

4.4.62 W. W. Heidbrink, *et al.*, Nucl. Fusion **46**, 324 (2006).

4.4.63 W. W. Heidbrink and G. J. Sadler, Nucl. Fusion **34**, 535 (1994).

4.4.64 S. S. Medley and A. L. Roquemore, Rev. Sci. Instrum. **75**, 3625 (2004).

4.4.65 J. E. Menard, *et al.*, Phys. Rev. Lett. **97**, 095022 (2006).

4.4.66 S. S. Medley, *et al.*, Nucl. Fusion **44**, (2004) 1158

4.4.67 S. S. Medley, *et al.*, "*Status of Recent Experimental and Analytical Investigation of MHD-Induced Energetic Ion Redistribution or Loss in the National Spherical Torus Experiment*" Princeton Plasma Physics Laboratory Report, PPPL-4235 (2007)

4.4.68 S. S. Medley, *et al.*, "*Neutral Particle Analyzer Vertically Scanning Measurements of MHD-Induced Energetic Ion Redistribution or Loss in the National Spherical Torus Experiment*," Princeton Plasma Physics Laboratory Report, PPPL-4270 (2007)